

Unsteady mixed flows in non uniform closed water pipes: a Full Kinetic Approach.

C. BOURDARIAS ^{*1}, M. ERSOY ^{†2,3} and S. GERBI^{‡1}

¹Laboratoire de Mathématiques, UMR 5127 - CNRS and Université de Savoie, 73376 Le Bourget-du-Lac Cedex, France.

²BCAM–Basque Center for Applied Mathematics, Bizkaia Technology Park 500, 48160, Derio, Basque Country, Spain.

³*Present address:* Université de Toulon, IMATH, EA 2134, 83957 La Garde, France.

Abstract

We recall the **PFS** (**P**ressurized and **F**ree **S**urface) model constructed for the modeling of unsteady mixed flows in closed water pipes where transition points between the free surface and pressurized flow are treated as a free boundary associated to a discontinuity of the gradient of pressure. Then we present a numerical kinetic scheme for the computations of unsteady mixed flows in closed water pipes. This kinetic method that we call FKA for “Full Kinetic Approach” is an easy and mathematically elegant way to deal with multiple transition points when the changes of state between free surface and pressurized flow occur. We use two approaches namely the “ghost waves approach” and the “Full Kinetic Approach” to treat these transition points. We show that this kinetic numerical scheme has the following properties: it is wet area conservative, under a CFL condition it preserves the wet area positive, it treats “naturally” the flooding zones and most of all it is very easy to implement it. Finally numerical experiments versus laboratory experiments are presented and the scheme produces results that are in a very good agreement. We also present a numerical comparison with analytic solutions for free surface flows in non uniform pipes: the numerical scheme has a very good behavior. A code to code comparison for pressurized flows is also conducted and leads to a very good agreement. We also perform a numerical experiment when flooding and drying flows may occur and finally make a numerical study of the order of the kinetic method.

Keywords: Mixed flows in closed water pipes, drying and flooding flows, kinetic interpretation of conservation laws, kinetic scheme with reflections.

AMS Subject classification : 65M08, 65M75, 76B07, 76M12, 76M28, 76N15

Notations concerning geometrical quantities

$\theta(x)$	angle of the inclination of the main pipe axis $z = Z(x)$ at position x
$\mathbf{Z}(t, x)$	dynamic topography
$\Omega(x)$	cross-section area of the pipe orthogonal to the axis $z = Z(x)$
$S(x)$	area of $\Omega(x)$
$R(x)$	radius of the cross-section $\Omega(x)$
$\sigma(x, z)$	width of the cross-section $\Omega(x)$ at altitude z

*Christian.Bourdarias@univ-savoie.fr

†Mehmet.Ersoy@univ-tln.fr

‡Stephane.Gerbi@univ-savoie.fr

Notations concerning the PFS model

$p(t, x, y, z)$	pressure
ρ_0	density of the water at atmospheric pressure p_0
$\rho(t, x, y, z)$	density of the water at the current pressure
$\bar{\rho}(t, x)$	$\bar{\rho}(t, x) = \frac{1}{S(x)} \int_{\Omega(x)} \rho(t, x, y, z) dy dz$ is the mean value of ρ over $\Omega(x)$ (press. flows)
c	sonic speed
$S_w(t, x)$	wet area i.e. part of the cross-section area in contact with water. $S_w = S(x)$ if the flow is pressurized
$A(t, x)$	$A(t, x) = \frac{\bar{\rho}(t, x)}{\rho_0} S_w(t, x)$ is the “equivalent wet area”. $S_w = A(t, x)$ if the flow is free surface
$u(t, x)$	velocity
$Q(t, x)$	$Q(t, x) = A(t, x)u(t, x)$ is the discharge
E	state indicator. $E = 0$ if the flow is free surface, $E = 1$ otherwise
$\mathcal{H}(S_w)$	the Z -coordinate of the water level equal to $\mathcal{H}(S_w) = h(t, x)$ if the state is free surface, $R(x)$ otherwise
$p(x, A, E)$	mean pressure over Ω
$K_s > 0$	Strickler coefficient depending on the material
$P_m(A)$	wet perimeter of A (length of the part of the channel section in contact with the water)
$R_h(A)$	$R_h(A) = \frac{A}{P_m(A)}$ is hydraulic radius

Bold characters are used for vectors, except for \mathbf{Z} , the dynamic topography defined later.

1 Introduction

The presented work takes place in a more general framework: the modeling of unsteady mixed flows in any kind of closed water pipes taking into account the cavitation problem and air entrapment. We are interested in flows occurring in closed pipes with non uniform sections, where some parts of the flow can be free surface (it means that only a part of the pipe is filled) and other parts are pressurized (it means that the pipe is full). The transition phenomenon between the two types of flows occurs in many situations such as storm sewers, waste or supply pipes in hydroelectric installations. It can be induced by sudden changes in the boundary conditions as failure pumping. During this process, the pressure can reach severe values and may cause damages. The simulation of such a phenomenon is thus a major challenge and a great amount of works was devoted to it these last years (see [12, 14, 30, 32], and references therein).

The classical shallow water equations are commonly used to describe free surface flows in open channels. They are also used in the study of mixed flows using the Preissman slot artefact (see for example [12, 32]). However, this technic does not take into account the subatmospheric pressurized flows (viewed as a free surface flow) which occur during a water hammer. In recent works, [19, 20, 21], a model for mixed flows in closed water pipes has been developed at University of Liège, where they use the artifact of the Preissman slot for supatmospheric pressurized flow and by introducing the concept of “negative Preissman slot” for subatmospheric pressurized flow. They proposed also a numerical scheme to compute the stationary flow, as well as the unsteady flow.

On the other hand the Allievi equations, commonly used to describe pressurized flows, are written in a non-conservative form which is not well adapted to a natural coupling with the shallow water equations.

A model for the unsteady mixed water flows in closed pipes, the **PFS** model, and a finite volume discretisation have been proposed by the authors in [4] and its mathematical derivation from the Euler incompressible equations (for the free surface part of the flow) and from the Euler isentropic compressible equations (for the pressurized part of the flow) is proposed in [6]. This model and the finite volume scheme extend the model studied by two of the authors for uniform pipes [8]. In [10] two of the authors has constructed a kinetic numerical scheme to compute pressurized flows in uniform pipes. For the case of a

non uniform closed pipe and for pressurized flow, the authors has extended the previous kinetic numerical scheme with reflections, see [3]. Let us also mention that the construction of a kinetic numerical scheme with a correct treatment of all the source terms has been published recently [5].

The paper is organized as follows. In the second section, we recall the **PFS** model and focus on the continuous flux whose gradient is discontinuous at the interface between free surface and pressurized flow. The source terms are also highlight: the conservative ones, the non conservative ones and the source term which is neither conservative nor conservative. We use the definition of the DLM theory [27] to define the non-conservative products. We state in this section the theoretical properties of the system that must be preserved by the numerical scheme.

Section 3 is devoted to the kinetic interpretation of the **PFS** model thanks to the classical kinetic interpretation of the system (see [29] for instance).

In section 4, we construct the kinetic scheme for the **PFS** model. The particular treatment of the friction term which is neither conservative nor non-conservative will be upwinded using the notion of *the dynamic topography*, already introduced by the authors in recent works [4, 5]. Firstly, we use the same kinetic scheme with reflections that we have constructed in [10, 3, 5] to treat the part of the flow where no transition points are present. Then we treat the transition points by two ways:

- as in [4], the “ghost waves approach” is used. We make an assumption on the speed of the discontinuity between free surface and pressurized flow, to compute the macroscopic states at the right hand side and the left hand side of this discontinuity. For this sake, we treat the transition points at the macroscopic level.
- a new approach that we called the “Full Kinetic Approach” is then used to treat these transition points. We stay at the microscopic level to build the macroscopic states at the right hand side and the left hand side of this discontinuity.

The particular treatment of the boundaries of the pipes is treated. Let us emphasize that the novelty in this work comes from the fact that the numerical scheme treats the transition points as well as the boundary conditions at the microscopic level so that a uniform approach is made possible.

In the last section, we present numerical experiments: the first one is the so-called Wiggert’s test where we have experimental data to compare with. A very good agreement is shown. Then we perform a code to code comparison for pressurized flow: we compare the results of the **belier** code used by the engineers of Electricité de France, Centre d’Ingénierie Hydraulique, Chambéry, (EDF-CIH) to compute a numerical solution of the Allievi equations by the characteristics method with the one we implemented, called **FlowMix**, for the same engineers for the computation of mixed flows.

Then we focus our attention in the numerical computations of steady states. This is due to the fact that we used of a very simple “maxwellian” function so that every computations of microscopic quantities are available exactly. This conducts to a very easy implementation of the numerical code which has the ambition to be exploited in an industrial way. Unfortunately, the use of such a function does not permit to prove mathematically that the numerical scheme permits the computations of steady states. Nethertheless, we compare the behavior of the numerical scheme towards the analytic transcritical steady solution of free surface flows in non uniform pipe: the results are in a very good agreement. Then a mixed “numerical” steady state is computed and again the numerical scheme shows a very good agreement. Moreover, let us say that this numerical scheme seems very robust since it is used “everyday” in an industrial way by the engineers of EDF-CIH in a lot of different configurations and they are confident in the numerical results. We will also test the robustness of the code **FlowMix** on a drying and flooding flow. The finite volume version of the method we have presented in [4] could not treat this type of flow unless by the introduction of a cut-off function that will produce a lack of conservation of mass. Finally we perform a numerical study of the order of the method on a unsteady mixed flow (computed by the VFRoe solver that we have constructed and validated in [4]) which will converge to a steady mixed flow.

In a similar framework, in [22], Euler equations for compressible fluids in a nozzle with variable discontinuous cross-section are considered. Regarding these equations as a nonconservative hyperbolic system,

weak solutions in the sense of Dal Maso, LeFloch and Murat [27] are investigated. A fully conservative entropy equality is derived and the authors construct well-balanced numerical scheme preserving the minimum entropy principle (see also [24, 23]).

For the sake of simplicity, we do not deal with the deformation of the domain induced by the change of pressure. We will consider only an infinitely rigid pipe (see [9] for unsteady pressurized flows in deformable closed pipe).

2 A model for unsteady water flows in closed water pipe

Although, in recent works (see [4, 6]), we have derived and studied a model for mixed flows in closed water pipes that we called the **PFS** model, for the sake of completeness of the present work, we briefly recall this model and its mathematical properties.

The **PFS** model (see [4, 6, 15]) is a mixed model of a pressurized (compressible) and free surface (incompressible) flow in a one dimensional rigid pipe with variable cross-section. The pressurized parts of the flow correspond to a full pipe whereas the section is not completely filled for the free surface flow.

The free surface part of the model is derived by writing the 3D Euler incompressible equations and by averaging over orthogonal sections to the privileged axis of the flow, the pressure being the hydrostatic pressure defined by:

$$P(t, x, z) = \rho_0 g (h(t, x) - z(x)) \cos \theta(x), \quad (1)$$

where g is the gravity constant, $\theta(x)$ the inclination of the pipe, ρ_0 is the density of the water at normal atmospheric conditions, $h(t, x)$ is the water height of the free surface whereas $z(x)$ is the altitude of the bottom of the pipe.

In the same spirit, by writing the Euler isentropic and compressible equations with the linearized pressure law

$$P(t, x, y, z) = p_0 + c^2 (\rho(t, x, y, z) - \rho_0), \quad (2)$$

where c the sonic speed of the water (assumed to be constant), ρ is the density of the water, we obtain a Saint-Venant like system of equations in the “FS-equivalent” variables $A(t, x) = \frac{\bar{p}(t, x)}{\rho_0} S(x)$, $Q(t, x) = A(t, x)u(t, x)$ which takes into account the compressible effects (for a detailed derivation, see [4, 6, 15]).

These variables are suitable to study mixed flows by setting:

$$A(t, x) = \frac{\bar{p}(t, x)}{\rho_0} S_w(t, x), \quad Q(t, x) = A(t, x)u(t, x),$$

where S_w is the *physical wet area*, i.e. the part of the cross-section area in contact with water.

In order to deal with the transition points (that is, when a change of state occurs), we introduce a state indicator variable E which is equal to 1 if the state is pressurized and to 0 if the state is free surface. Notice that S_w is (A, E) dependent via the relations:

$$S_w = S_w(A, E) = \begin{cases} S & \text{if } E = 1, \\ A & \text{if } E = 0. \end{cases}$$

After taking the mean value of the pressure term in the Euler equations over the wetted cross-section, we get the pressure law as a mixed “hydrostatic” (for the free surface part of the flow) and “acoustic” type (for the pressurized part of the flow) as follows:

$$p(x, A, E) = c^2(A - S_w) + gI_1(x, S_w) \cos \theta. \quad (3)$$

Thus the continuity is obtained by the “artificial” addition in the pressure law of the term $-c^2 S_w$. This form of the pressure insures the continuity of it at transition points.

The term I_1 is the classical hydrostatic pressure:

$$I_1(x, S_w) = \int_{-R}^{\mathcal{H}(S_w)} (\mathcal{H}(S_w) - z)\sigma dz,$$

where $\sigma(x, z)$ is the width of the cross-section, $R = R(x)$ the radius of the cross-section and $\mathcal{H}(S_w)$ is the z -coordinate of the free surface over the main axis $Z(x)$ (see figure 1 and figure 2).

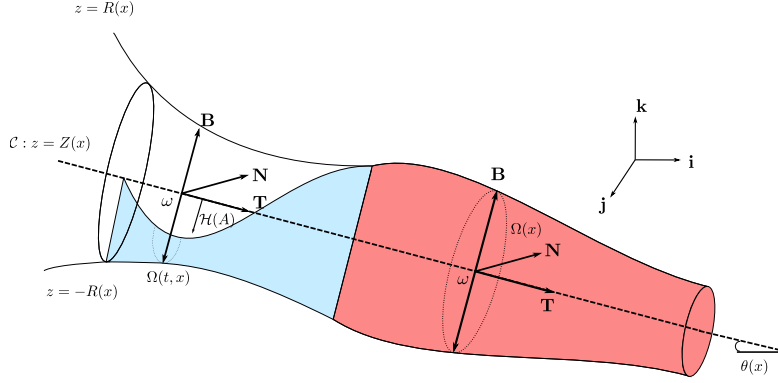


Figure 1: Geometric characteristics of the domain: free surface and pressurized flow.

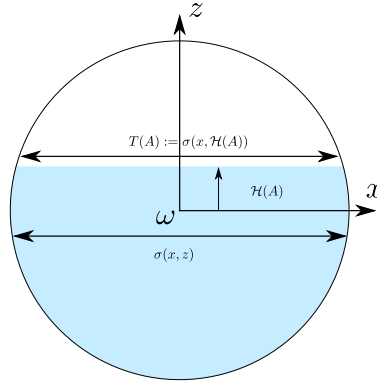


Figure 2: Cross-section Ω .

Remark 2.1. We can also regard $I_1/A = \bar{y}$ as the distance separating the free surface to the center of the mass of the wet section (see figure 3).

The pressure defined by Equation (3) is continuous throughout the transition points and we define the PFS model by:

$$\begin{cases} \partial_t(A) + \partial_x(Q) & = 0, \\ \partial_t(Q) + \partial_x\left(\frac{Q^2}{A} + p(x, A, E)\right) & = -gAZ' + Pr(x, A, E) \\ & -G(x, A, E) \\ & -K(x, A, E)\frac{Q|Q|}{A}. \end{cases} \quad (4)$$

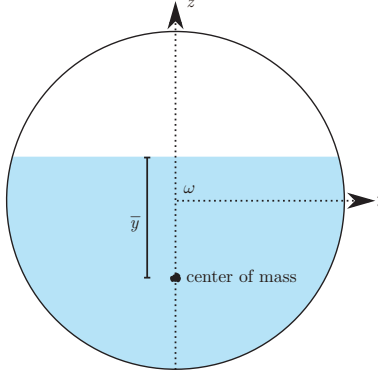


Figure 3: The distance separating the free surface to the center of the mass of the wet section.

where $x \in (0, L)$, L being the length of the pipe, $z = Z(x)$ is the altitude of the main pipe axis. The terms Pr , G and K denote respectively the pressure source term, a curvature term and the friction:

$$\begin{aligned} Pr(x, A, E) &= c^2 (A - S_w) \frac{S'}{S_w} + g I_2(x, S_w) \cos \theta, \\ G(x, A, E) &= g A \bar{Z}(x, S_w) (\cos \theta)' = g A (\mathcal{H}(S_w) - I_1(x, S_w)/S_w) (\cos \theta)', \\ K(x, A, E) &= \frac{1}{K_s^2 R_h(S_w)^{4/3}}, \end{aligned}$$

where we have used the notation f' to denote the derivative with respect to the space variable x of any function $f(x)$. The term I_2 is the hydrostatic pressure source term defined by:

$$I_2(x, S_w) = \int_{-R}^{\mathcal{H}(S_w)} (\mathcal{H}(S_w) - z) \partial_x \sigma dz.$$

The term $K_s > 0$ is the Strickler coefficient depending on the material and $R_h(S_w)$ is the hydraulic radius.

Remark 2.2. *Let us remark that whenever S is constant on a sub-interval of $(0, L)$, that is σ is constant, then $I_2(x, S_w) = 0$. This fact will be used in the kinetic interpretation of the **PFS** equations.*

Remark 2.3. *For the sake of clarity, let us detail the different terms of equation (4) for a free surface flow and a pressurized one.*

- For a free surface flow, we have:

$$\begin{aligned} p(x, A, 0) &= g I_1(x, A) \cos \theta, \\ Pr(x, A, 0) &= g I_2(x, A) \cos \theta, \\ G(x, A, 0) &= g A \bar{Z}(x, A) (\cos \theta)', \\ K(x, A, 0) &= \frac{1}{K_s^2 R_h(A)^{4/3}}. \end{aligned}$$

- For a pressurized flow, we have:

$$\begin{aligned} p(x, A, 1) &= c^2 (A - S(x)) + g I_1(x, S(x)) \cos \theta, \\ Pr(x, A, 1) &= c^2 (A - S(x)) \frac{S'(x)}{S(x)} + g I_2(x, S(x)) \cos \theta, \\ G(x, A, 1) &= g A \bar{Z}(x, S(x)) (\cos \theta)', \\ K(x, A, 1) &= \frac{1}{K_s^2 R_h(S(x))^{4/3}}. \end{aligned}$$

Let us notice that in this case, the term $c^2(A - S(x))$ in $p(x, A, 1)$ represents the over-pressure.

Remark 2.4. The unknown state vector is denoted $\mathbf{U} = (A, Q)$ and the flux vector \mathbf{F} by:

$$\mathbf{F}(x, \mathbf{U}, E) = \left(Q, \frac{Q^2}{A} + p(x, A, E) \right).$$

We simply denote (when no ambiguity is possible):

$$F_2(A, Q) = \frac{Q^2}{A} + p(x, A, E), \quad (5)$$

the second component of the preceding flux.

As it was pointed out in [4, Remark 4.2], the flux is continuous through the change of state of the flow whereas its derivative with respect to A is discontinuous, due to the jump of the sound speed, see figure 4.

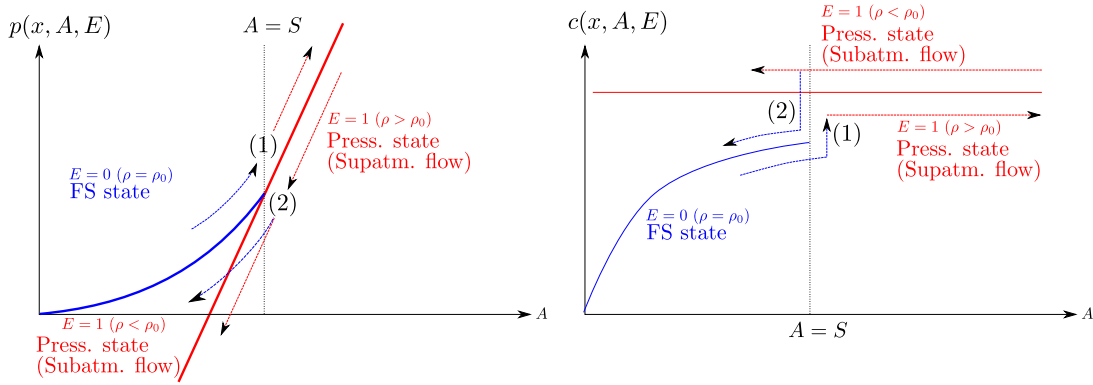


Figure 4: Pressure law and sound speed $c(x, A, E)$ in the case of a rectangular pipe. Trajectory (1) corresponds to a pressurization. Trajectory (2) depends on the state of the flow around

Identification of the source terms.

In order to write the kinetic interpretation of the **PFS** equations, we have to factorize by A the right hand side of System (4). Then, the source terms reads as follows:

- gZ' is a conservative term.
- $c^2 \left(\frac{A - S_w}{AS_w} \right) S' = \begin{cases} c^2 \left(\frac{A - S}{A} \right) \frac{S'}{S} & \text{if } E = 1 \\ 0 & \text{if } E = 0 \end{cases}$ is a non-conservative product.
- $g \frac{I_2(x, S_w) \cos \theta}{A}$ is neither conservative nor non-conservative.
- $g \bar{Z}(x, S_w) (\cos \theta)' = g (\mathcal{H}(S_w) - I_1(x, S_w)/S_w) \cos \theta'$ is a non-conservative product.
- $K(x, A, E) \frac{Q|Q|}{A^2}$ is neither conservative nor non-conservative.

Moreover, all the terms said to be non-conservative products are genuinely non-conservative product since they do not write as an exact differential form.

System (4) has the following properties:

Theorem 2.1.

1. System (4) is strictly hyperbolic on $\{A(t, x) > 0\}$.
2. For smooth solutions, the mean velocity $u = Q/A$ satisfies:

$$\partial_t u + \partial_x \left(\frac{u^2}{2} + c^2 \ln(A/S_w) + g\mathcal{H}(S_w) \cos \theta + gZ \right) = -gK(x, A, E)u|u| \leq 0. \quad (6)$$

The quantity $\Phi(A, Q, \cos \theta, Z, E) = \frac{u^2}{2} + c^2 \ln(A/S_w) + g\mathcal{H}(S_w) \cos \theta + gZ$ is called the total head.

3. The still water steady state, for $u = 0$, reads:

$$c^2 \ln(A/S_w) + g\mathcal{H}(S_w) \cos \theta + gZ = cte, \quad (7)$$

for some constant cte .

4. System (4) admits a mathematical entropy:

$$\mathcal{E}(A, Q, E) = \frac{Q^2}{2A} + c^2 A \ln(A/S_w) + c^2 S + gA\bar{Z}(x, S_w) \cos \theta + gAZ,$$

which satisfies the entropy relation for smooth solutions

$$\partial_t \mathcal{E} + \partial_x ((\mathcal{E} + p(x, A, E))u) = -gAK(x, A, E)u^2|u| \leq 0. \quad (8)$$

Proof. The proof of these assumptions relies only on algebraic combinations of the two equations forming System (4) and is left to the reader. \square

In what follows, when no confusion is possible, the term $K(x, A, E)$ will be denoted simply $K(x, A)$ for free surface states and $K(x, S)$ for pressurized states.

Remark 2.5. Equation (7) is the still water steady state equation associated to the **PFS** equation. Indeed, for a pressurized flow (i.e. $S_w = S$), when $u = 0$ and $A = A(x)$, the following equation holds:

$$c^2 \ln(A/S) + g\mathcal{H}(S) \cos \theta + gZ = cte.$$

Moreover when $S_w = A$, Equation (7) provides $g\mathcal{H}(A) \cos \theta + gZ = cte$: this equation represents the horizontal line for a free surface still water steady states. Moreover, when mixed still water steady states occur, i.e. when one part of the flow is pressurized and the other part of the flow is free surface, Equation (7) holds again.

3 The kinetic interpretation of the PFS model

Recently in [4], we have investigated a class of approximated Godunov scheme for the present **PFS** model in which we show how to obtain by a suitable definition of the convection matrix an exactly well-balanced scheme for the still water steady state. We also point out that the upwinding of the source terms into the numerical fluxes introduces a stationary wave with a vanishing denominator. We also discuss on the possibility to introduce a cut-off function to avoid the division by zero. But, the truncation of the wet area A induces a loss of mass which implies a loss of the conservativity property. Moreover, the numerical scheme loses accuracy. Therefore, stationary hydraulic jump and flooding area are not accurately computed with this kind of numerical scheme. As pointed out in [29], the numerical kinetic scheme are proved to satisfy

the following stability properties: the water height conservativity, the in cell entropy inequality and the conservation of the still water steady state. Unfortunately, it holds only for rectangular geometry.

The goal of this paper is to construct a Finite Volume-Kinetic scheme that preserves the wetted area positive, that can treat naturally the flooding and also that is easily implemented.

The big challenge in this construction is the fact that the continuous flux has a discontinuous gradient at the interface between free surface and pressurized flow, see Remark 2.4. In [4], the finite volume scheme that we have constructed uses the “ghost waves approach” to overcome this difficulty. We will see that we can still use this approach for the finite volume kinetic scheme but we will prefer to construct a fully kinetic scheme that is a scheme at the kinetic level which treats the changes of type of the flow.

First of all, let us recall the kinetic interpretation of the **PFS** model based on Perthame’s kinetic formulation of conservation laws [28].

3.1 The mathematical kinetic interpretation

Let $\chi : \mathbb{R} \rightarrow \mathbb{R}$ be a given real function satisfying the following properties:

$$\chi(\omega) = \chi(-\omega) \geq 0, \quad \int_{\mathbb{R}} \chi(\omega) d\omega = 1, \quad \int_{\mathbb{R}} \omega^2 \chi(\omega) d\omega = 1. \quad (9)$$

It permits to define the density of particles, by a so-called *Gibbs equilibrium*,

$$\mathcal{M}(t, x, \xi) = \frac{A(t, x)}{b(t, x)} \chi\left(\frac{\xi - u(t, x)}{b(t, x)}\right), \quad (10)$$

where $b(t, x) = b(x, A(t, x), E(t, x))$ with

$$b(x, A, E) = \begin{cases} \sqrt{g \frac{I_1(x, A)}{A} \cos \theta} & \text{if } E = 0, \\ \sqrt{g \frac{I_1(x, S)}{A} \cos \theta + c^2} & \text{if } E = 1. \end{cases} \quad (11)$$

Remark 3.1. *Let us remark that when $E = 0$, we have $b(x, A, 0) = \sqrt{G\bar{y} \cos \theta}$, where \bar{y} is the distance separating the free surface to the center of the mass of the wet section (see figure 3).*

The Gibbs equilibrium \mathcal{M} is related to the **PFS** model by the classical *macro-microscopic* kinetic relations:

$$A = \int_{\mathbb{R}} \mathcal{M}(t, x, \xi) d\xi, \quad (12)$$

$$Q = \int_{\mathbb{R}} \xi \mathcal{M}(t, x, \xi) d\xi, \quad (13)$$

$$\frac{Q^2}{A} + A b(x, A, E)^2 = \int_{\mathbb{R}} \xi^2 \mathcal{M}(t, x, \xi) d\xi. \quad (14)$$

From the relations (12)–(14), the nonlinear **PFS** model can be viewed as a single linear equation involving the nonlinear quantity \mathcal{M} :

Theorem 3.1 (Kinetic interpretation of the **PFS** model). *(A, Q) is a strong solution of System (4) if and only if \mathcal{M} satisfies the kinetic transport equation:*

$$\partial_t \mathcal{M} + \xi \cdot \partial_x \mathcal{M} - g\phi \partial_\xi \mathcal{M} = \mathcal{K}(t, x, \xi), \quad (15)$$

for a collision term $\mathcal{K}(t, x, \xi)$ which satisfies for (t, x) a.e.

$$\int_{\mathbb{R}} \begin{pmatrix} 1 \\ \xi \end{pmatrix} \mathcal{K}(t, x, \xi) d\xi = 0,$$

where the source term ϕ is defined as:

$$\begin{aligned} \text{if } E = 0, \quad \phi(x) &= \partial_x Z + K(x, A)u|u| - \frac{I_2(x, A) \cos \theta}{A} + \bar{Z}(x, A)\partial_x \cos \theta, \\ \text{if } E = 1, \quad \phi(x) &= \partial_x Z + K(x, S)u|u| - \frac{I_2(x, S) \cos \theta}{A} - \frac{c^2}{g} \frac{A - S}{A} \frac{\partial_x S}{S} + \bar{Z}(x, S)\partial_x \cos \theta. \end{aligned} \quad (16)$$

Proof. The proof relies on very obvious computations since \mathcal{M} verifies the macro-microscopic kinetic relations (12), (13), (14), and from the definition of the source terms ϕ . \square

Remark 3.2. *The kinetic interpretation presented in Theorem 3.1 is a (non physical) microscopic description of the PFS model.*

4 Construction of the kinetic scheme for the PFS model

In this section, following the works of [29, 5], we will construct a finite volume kinetic scheme that preserves the wetted area positive and that will compute “naturally” flooding zones. The main feature of this scheme is the treatment of transition points between free surface and pressurized flows. In a first step, we will use the “ghost waves approach” that we have constructed in [4] to treat this difficulty: to this end we will go back to the macroscopic level to compute the unknown states (A, Q) at the interface between free surface and pressurized flow.

In a second step, we will construct a fully kinetic scheme to treat the interface between the free surface and the pressurized flow: the Gibbs equilibrium on the right hand side and the left hand side of the interface between free surface and pressurized flow will be computed by kinetic formulas. To upwind all the source terms at the microscopic level, we will use the ideas presented in the recent work of the authors [5].

The particular treatment of the boundary conditions only at the microscopic level will be rapidly exposed. This is the key feature of the “Full Kinetic Approach”.

4.1 The kinetic scheme without transition points

In this section, we will treat the parts of the flow that are either free surface or pressurized. Under this assumption and based on the kinetic interpretation (see Theorem 3.1), we construct easily a Finite Volume scheme where the conservative quantities are cell-centered and source terms are included into the numerical fluxes by a standard kinetic scheme with reflections [29].

To this end, let $N \in \mathbb{N}^*$, and let us consider the following mesh on $[0, L]$. Cells are denoted for every $i \in [0, N + 1]$, by $m_i = (x_{i-1/2}, x_{i+1/2})$, with $x_i = \frac{x_{i-1/2} + x_{i+1/2}}{2}$ and $h_i = x_{i+1/2} - x_{i-1/2}$ the space step. The “fictitious” cells m_0 and m_{N+1} denote the boundary cells and the mesh interfaces located at $x_{1/2}$ and $x_{N+1/2}$ are respectively the upstream and the downstream ends of the pipe (see figure 5).

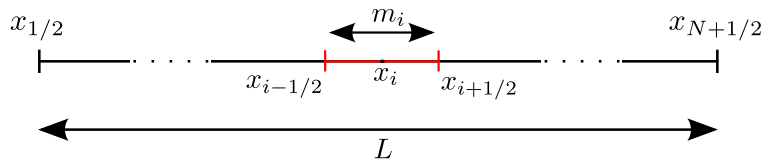


Figure 5: The space discretisation.

We also consider a time discretization t^n defined by $t^{n+1} = t^n + \Delta t^n$ with Δt^n the time step.

We denote $\mathbf{U}_i^n = (A_i^n, Q_i^n)$, $u_i^n = \frac{Q_i^n}{A_i^n}$, \mathcal{M}_i^n the cell-centered approximation of $\mathbf{U} = (A, Q)$, u and \mathcal{M} on the cell m_i at time t^n . We denote by $\mathbf{U}_0^n = (A_0^n, Q_0^n)$ the upstream and $\mathbf{U}_{N+1}^n = (A_{N+1}^n, Q_{N+1}^n)$ the downstream state vectors.

For $i \in [0, N+1]$, E_i is the state indicator of the cell: $E_i = 0$ if in the cell m_i , the flow is a free surface flow, $E_i = 1$ if in the cell m_i , the flow is a pressurized flow.

On a time interval $[t^n, t^{n+1}]$ and on the cell m_i , the kinetic equation (15) writes:

$$\begin{cases} \partial_t \mathcal{M} + \xi \cdot \partial_x \mathcal{M} - g\phi \partial_\xi \mathcal{M} = \mathcal{K}(t, x, \xi) & \text{for } x \in m_i, t \in (t^n, t^{n+1}), \xi \in \mathbb{R}, \\ \mathcal{M}(t^n, x, \xi) = \mathcal{M}_i^n(\xi) & \text{for } x \in m_i, \xi \in \mathbb{R}. \end{cases} \quad (17)$$

Remark 4.1. *At this stage, for $x \in m_i$, it is convenient to introduce the term:*

$$\mathbf{Z}_i(t, x) = \left(Z(x) + \int_{x_{i-1/2}}^x K(s, A(t, s), E) u(t, s) |u(t, s)| ds \right),$$

which is called **the dynamic topography** since it is time and space variable dependent contrary to the **static topography** Z which is only x -dependent. This notion is closely related to the ‘‘apparent topography’’ introduced by Bouchut et al [1, 2, 26].

For $x \in m_i$, denoting

$$\mathbf{W} = (\mathbf{Z}_i, S, \cos \theta), \quad (18)$$

the source term ϕ defined by (16) becomes:

$$\begin{aligned} \text{if } E = 0, \quad \phi(x, \mathbf{W}) &= \partial_x \mathbf{Z}_i - \frac{I_2(x, A) \cos \theta}{A} + \bar{Z}(x, A) \partial_x \cos \theta, \\ \text{if } E = 1, \quad \phi(x, \mathbf{W}) &= \partial_x \mathbf{Z}_i - \frac{I_2(x, S) \cos \theta}{A} - \frac{c^2}{g} \frac{A - S}{A} \frac{\partial_x S}{S} + \bar{Z}(x, S) \partial_x \cos \theta. \end{aligned} \quad (19)$$

The piecewise constant representation of \mathbf{W} defined by (18) is given by, $\mathbf{W}(t, x) = \mathbf{W}_i(t) \mathbf{1}_{m_i}(x)$ where $\mathbf{W}_i(t)$ is defined as $\mathbf{W}_i(t) = \frac{1}{\Delta x} \int_{m_i} \mathbf{W}(t, x) dx$ for instance.

Remark 4.2. *Let us notice that as $\mathbf{W}(x, t) = \mathbf{W}_i(t)$ is constant on the cell m_i , thanks to remark 2.2, $\phi(x, \mathbf{W}) = 0$ on the cell m_i . Indeed, since \mathbf{Z}_i is constant, $\partial_x \mathbf{Z}_i = 0$, since S is constant, $I_2(x, S_w) = 0$ and $\partial_x S = 0$ and since θ is constant, $\partial_x \cos \theta = 0$.*

We use this simple fact to construct the kinetic scheme as follows.

Neglecting the collision kernel as in [29, 5] the kinetic transport equation (17) simply reads:

$$\begin{cases} \frac{\partial}{\partial t} f + \xi \cdot \frac{\partial}{\partial x} f = 0 & \text{for } x \in m_i, t \in (t^n, t^{n+1}), \xi \in \mathbb{R}, \\ f(t^n, x, \xi) = \mathcal{M}_i^n(\xi) & \text{for } x \in m_i, \xi \in \mathbb{R}. \end{cases} \quad (20)$$

This equation is a linear transport equation whose explicit discretisation may be done directly by the following way. A finite volume discretisation of Equation (20) leads to:

$$\forall \xi \in \mathbb{R}, \forall x \in m_i, f(t^{n+1}, x, \xi) = f_i^{n+1}(\xi) = \mathcal{M}_i^n(\xi) + \frac{\Delta t}{h_i} \xi \left(\mathcal{M}_{i+\frac{1}{2}}^-(\xi) - \mathcal{M}_{i-\frac{1}{2}}^+(\xi) \right), \quad (21)$$

where the fluxes $\mathcal{M}_{i+\frac{1}{2}}^\pm$ have to take into account the discontinuity of the source term $\phi(x, \mathbf{W})$ at the cell interface $x_{i+1/2}$. This is the principle of interfacial source upwind. Indeed, noticing that the fluxes can also be written as:

$$\mathcal{M}_{i+\frac{1}{2}}^-(\xi) = \mathcal{M}_{i+\frac{1}{2}} + \left(\mathcal{M}_{i+\frac{1}{2}}^- - \mathcal{M}_{i+\frac{1}{2}} \right),$$

the quantity $\delta\mathcal{M}_{i+\frac{1}{2}}^- = \mathcal{M}_{i+\frac{1}{2}}^- - \mathcal{M}_{i+\frac{1}{2}}^+$ holds for the discrete contribution of the source term $\phi(x, \mathbf{W})$ in the system for negative velocities $\xi \leq 0$ due to the upwinding of the source term. Thus $\delta\mathcal{M}_{i+\frac{1}{2}}^-$ has to vanish for positive velocity $\xi > 0$, as proposed by the choice of the interface fluxes below. Let us now detail our choice for the fluxes $\mathcal{M}_{i+\frac{1}{2}}^\pm$ at the interface. It can be justified by using a generalized characteristic method for Equation (15) (without the collision kernel) but we give instead a presentation based on some physical energetic balance. The details of the construction of these fluxes by the general characteristics method (see [13, Definition 2.1]) is done in [15, Chapter 2].

In order to take into account the neighboring cells by means of a natural interpretation of the microscopic features of the system, we formulate a peculiar discretisation for the fluxes in (21), computed by the following upwinded formulas:

$$\begin{aligned}
\mathcal{M}_{i+1/2}^-(\xi) &= \overbrace{\mathbb{1}_{\{\xi>0\}}\mathcal{M}_i^n(\xi)}^{\text{positive transmission}} + \overbrace{\mathbb{1}_{\{\xi<0,|\xi|^2-2g\phi_{i+1/2}^n<0\}}\mathcal{M}_i^n(-\xi)}^{\text{reflection}} \\
&+ \underbrace{\mathbb{1}_{\{\xi<0,|\xi|^2-2g\phi_{i+1/2}^n>0\}}\mathcal{M}_{i+1}^n\left(-\sqrt{|\xi|^2-2g\phi_{i+1/2}^n}\right)}_{\text{negative transmission}}, \\
\mathcal{M}_{i+1/2}^+(\xi) &= \overbrace{\mathbb{1}_{\{\xi<0\}}\mathcal{M}_{i+1}^n(\xi)}^{\text{negative transmission}} + \overbrace{\mathbb{1}_{\{\xi>0,|\xi|^2+2g\phi_{i+1/2}^n<0\}}\mathcal{M}_{i+1}^n(-\xi)}^{\text{reflection}} \\
&+ \underbrace{\mathbb{1}_{\{\xi>0,|\xi|^2+2g\phi_{i+1/2}^n>0\}}\mathcal{M}_i^n\left(\sqrt{|\xi|^2+2g\phi_{i+1/2}^n}\right)}_{\text{positive transmission}}.
\end{aligned} \tag{22}$$

The term $\phi_{i\pm 1/2}^n$ in (22) is the upwinded source term (16). It also plays the role of the potential barrier: the term $|\xi|^2 \pm 2g\phi_{i+1/2}^n$ is the jump condition for a particle with a kinetic speed ξ which is necessary to

- be reflected: this means that the particle has not enough kinetic energy $|\xi|^2/2$ to overpass the potential barrier (reflection term in (22)),
- overpass the potential barrier with a positive speed (positive transmission term in (22)),
- overpass the potential barrier with a negative speed (negative transmission term in (22)).

Having in mind the so-called non conservative products defined by Dal Maso, Murat and Lefloch [27], and recalling that the dynamic topography is defined on the cell m_i as $\mathbf{Z}_i(t, x) = \left(Z(x) + \int_{x_{i-1/2}}^x K(s, A, E)u|u| ds \right)$, we choose a midpoint approximation of the source term ϕ defined by Equation (16) at the interface x_i . The same “trick” is used to take into account the pressure source term involving $I_2(x, S_w)$ that is :

$$I_2(x, S_w) = \frac{\partial}{\partial x} \left(\int_{x_{i-1/2}}^x I_2(s, S_w) ds \right).$$

Thus, the potential barrier $\phi_{i+1/2}^n$ has the following expression:

$$\begin{aligned}
\text{if } E = 0, \phi_{i+\frac{1}{2}}^n &= Z_{i+1} - Z_i \\
&+ \frac{h_i}{2} K(x_i, A_i^n, E_i^n) u_i^n |u_i^n| + \frac{h_{i+1}}{2} K(x_{i+1}, A_{i+1}^n, E_{i+1}^n) u_{i+1}^n |u_{i+1}^n| \\
&- \left(\frac{h_i}{2} \frac{I_2(x_i, A_i) \cos \theta_i}{A_i} + \frac{h_{i+1}}{2} \frac{I_2(x_{i+1}, A_{i+1}) \cos \theta_{i+1}}{A_{i+1}} \right) \\
&+ \frac{\bar{Z}_i^n + \bar{Z}_{i+1}^n}{2} (\cos \theta_{i+1} - \cos \theta_i),
\end{aligned}$$

$$\begin{aligned}
\text{if } E = 1, \phi_{i+\frac{1}{2}}^n &= Z_{i+1} - Z_i \\
&+ \frac{h_i}{2} K(x_i, A_i^n, E_i^n) u_i^n |u_i^n| + \frac{h_{i+1}}{2} K(x_{i+1}, A_{i+1}^n, E_{i+1}^n) u_{i+1}^n |u_{i+1}^n| \\
&- \left(\frac{h_i}{2} \frac{I_2(x_i, S(x_i)) \cos \theta_i}{A_i} + \frac{h_{i+1}}{2} \frac{I_2(x_{i+1}, S(x_{i+1})) \cos \theta_{i+1}}{A_{i+1}} \right) \\
&- \frac{c^2}{g} \left(\frac{1}{2} \frac{(A_i - S(x_i))}{A_i} + \frac{1}{2} \frac{(A_{i+1} - S(x_{i+1}))}{A_{i+1}} \right) \left(\ln(S(x_{i+1})) - \ln(S(x_i)) \right) \\
&+ \frac{\bar{Z}_i^n + \bar{Z}_{i+1}^n}{2} (\cos \theta_{i+1} - \cos \theta_i).
\end{aligned}$$

As the first term of $\phi_{i+\frac{1}{2}}^n$ is $Z_{i+1} - Z_i$, we recover the classical interfacial upwinding for the conservative term Z used by Perthame and Simeoni [29].

Since we neglect the collision term, it is clear that f^{n+1} computed by the discretised kinetic equation (21) is no more a Gibbs equilibrium. Therefore, to recover the macroscopic variables A and Q , according to the identities (12)-(13), we set:

$$\mathbf{U}_i^{n+1} = \begin{pmatrix} A_i^{n+1} \\ Q_i^{n+1} \end{pmatrix} \stackrel{def}{=} \int_{\mathbb{R}} \begin{pmatrix} 1 \\ \xi \end{pmatrix} f_i^{n+1} d\xi.$$

In fact at each time step, we projected $f^n(\xi)$ on $\mathcal{M}_i^n(\xi)$, which is a way to perform all collisions at once and to recover a Gibbs equilibrium without computing it.

Now, we can integrate the discretised kinetic equation (21) against 1 and ξ to obtain the macroscopic kinetic scheme:

$$\mathbf{U}_i^{n+1} = \mathbf{U}_i^n + \frac{\Delta t^n}{h_i} \left(\mathbf{F}_{i+\frac{1}{2}}^- - \mathbf{F}_{i-\frac{1}{2}}^+ \right). \quad (23)$$

The numerical fluxes are thus defined by the kinetic fluxes as follows:

$$\mathbf{F}_{i+\frac{1}{2}}^\pm \stackrel{def}{=} \int_{\mathbb{R}} \xi \begin{pmatrix} 1 \\ \xi \end{pmatrix} \mathcal{M}_{i+\frac{1}{2}}^\pm(\xi) d\xi. \quad (24)$$

At this stage of the construction of the scheme, the choice of the function χ is crucial. The two main features of this choice are the following:

- the numerical kinetic scheme should preserve the still water steady state $u = 0$ which gives equation (7). Writing the kinetic formulation of the still water steady state, we obtain an ordinary differential equation for the function χ which looks like equation (16) in the work of Perthame and Simeoni [29] with additional terms. For a non uniform pipe, we are not able to find an explicit solution of this ordinary differential equation.
- the numerical scheme should also exhibit an in cell entropy inequality. This fact may be obtained for a function χ that minimizes a kinetic energy. Unfortunately, as pointed out in the work of Bourdarias *et al.* [11, Equation (24)], for a pressurized flow in a uniform pipe, the function χ that minimizes the kinetic energy has a non compact support. In the same work, the authors had noticed that the kinetic energy for a free surface flow is not always convex [11, Remark 7].

Nevertheless, as done by the authors in [4, Equations (55)-(56)], a well balanced corrections may be implemented at the macroscopic level to recover the still water steady state. This is not the goal of the present work.

In this work, we have chosen a compact support function χ in order to fulfill a CFL type condition to obtain a scheme that preserves the positivity of the wet area and therefore to ensure the L^∞ stability of the scheme. Moreover, every annoying computations of integrals involving the function χ will lead to exact and easy computations.

For the direct computations of all integral terms, we have chosen in the industrial code `FlowMix` (used by the engineers of Electricité de France, Centre d'Ingénierie Hydraulique, Chambéry):

$$\chi = \frac{1}{2\sqrt{3}} \mathbb{1}_{[-\sqrt{3}, \sqrt{3}]} . \quad (25)$$

Let us emphasize that although the function χ chosen for the computations does not lead to the preservation of steady states and to the in cell entropy inequality, the numerical results presents in section 5.3 show a very good behavior of the numerical kinetic scheme to recover free surface steady state as well as mixed steady states without notable damages.

Proposition 4.1. *Let χ be a compactly supported function verifying (9) and denote $[-M, M]$ its support. The kinetic scheme (23)-(24) has the following properties:*

1. *The kinetic scheme is a wet area conservative scheme,*
2. *Assume the following CFL condition*

$$\Delta t^n \max_i (|u_i^n| + M b_i^n) \leq \max_i h_i \quad (26)$$

holds. Then the kinetic scheme keeps the wet area A positive i.e.:

$$\text{if, for every } i \in [0, N + 1], A_i^0 \geq 0 \text{ then, for every } i \in [0, N + 1], A_i^n \geq 0.$$

3. *The kinetic scheme treats “naturally” flooding zones.*

Proof. We will adapt the proof of [29] to show the three properties that verify the kinetic scheme.

1. Let us denote the first component of the discrete fluxes (24) $(F_A)_{i+\frac{1}{2}}^\pm$:

$$(F_A)_{i+\frac{1}{2}}^\pm \stackrel{\text{def}}{=} \int_{\mathbb{R}} \xi \mathcal{M}_{i+\frac{1}{2}}^\pm(\xi) d\xi$$

An easy computation, using the change of variable $\mu = |\xi|^2 - 2g\phi_{i+\frac{1}{2}}^n$, allows us to show that:

$$(F_A)_{i+\frac{1}{2}}^+ = (F_A)_{i+\frac{1}{2}}^- .$$

2. Suppose that for every $i \in [0, N + 1], A_i^n > 0$. Let us denote $\xi_\pm = \max(0, \pm\xi)$ and $\sigma = \frac{\Delta t^n}{\max_i h_i}$. From Equation (21), we get the following equation:

$$\begin{aligned} f_i^{n+1}(\xi) &= (1 - \sigma|\xi|) \mathcal{M}_i^n(\xi) \\ &+ \sigma \xi_+ \left[\mathbb{1}_{\{|\xi|^2 + 2g\Delta\phi_{i+1/2} < 0\}} \mathcal{M}_i^n(-\xi) \right. \\ &\left. + \mathbb{1}_{\{|\xi|^2 + 2g\Delta\phi_{i-1/2} > 0\}} \mathcal{M}_{i-1}^n \left(\sqrt{|\xi|^2 + 2g\Delta\phi_{i+1/2}} \right) \right] \\ &+ \sigma \xi_- \left(\mathbb{1}_{\{|\xi|^2 - 2g\Delta\phi_{i+1/2} < 0\}} \mathcal{M}_i^n(-\xi) \right. \\ &\left. + \mathbb{1}_{\{|\xi|^2 - 2g\Delta\phi_{i-1/2} > 0\}} \mathcal{M}_{i+1}^n \left(-\sqrt{|\xi|^2 - 2g\Delta\phi_{i+1/2}} \right) \right) . \end{aligned}$$

Since the function χ is compactly supported if $|\xi - u_i^n| \geq M b_i^n$ then $\mathcal{M}_i^n(\xi) = 0$. Thus

$$f_i^{n+1}(\xi) \geq 0 \text{ if } |\xi - u_i^n| \geq M b_i^n ,$$

as a sum of non negative terms.

On the other hand, for $|\xi - u_i^n| \leq M b_i^n$, using the CFL condition $0 < \sigma |\xi| \leq 1$, for all i , $f_i^{n+1} \geq 0$ since it is a convex combination of non negative terms.

Finally we have $\forall i \in [0, N + 1]$, $f_i^n \geq 0$. Since $\forall i \in [0, N + 1]$, $A_i^{n+1} = \int_{\mathbb{R}} f_i^{n+1}(\xi) d\xi$, we finally get $\forall i \in [0, N + 1]$, $A_i^{n+1} \geq 0$.

3. Suppose $A_i^n = 0$. Of course, in the mesh i the flow is a free surface flow. So using the definition of \mathcal{M} , and the fact that the function χ is compactly supported, the only term that may cause problem is $\frac{A}{b(t, x)}$.

But since when $E = 0$, we have (thanks to Remark 3.1):

$$\frac{A}{b(t, x)} = \sqrt{\frac{A}{g\bar{y} \cos \theta}}.$$

Thus, for all the usual pipe geometries (rectangular, trapezoidal, circular, ...) an easy computation gives:

$$\lim_{\substack{A \rightarrow 0 \\ A \geq 0}} \frac{A}{b(t, x)} = 0.$$

Otherwise, we add as an assumption that for the considered pipe geometry, we suppose that:

$$\lim_{\substack{A \rightarrow 0 \\ A \geq 0}} \sqrt{\frac{A}{\bar{y}}} = 0.$$

Therefore, we get $\mathcal{M}_i^n(\xi) = 0$. This is the reason why we say that the kinetic scheme treats “naturally” the flooding zones. □

4.2 The kinetic scheme with transition points

The transition points are characterized by the points of the pipe where the flow is not of the same type on the left hand side and the right hand side of these points. More precisely, they are characterized by their localization in the pipe and the speed of propagation w of the change of the state. We will assume that it exists at most a finite set of transition points and we will consider that these transition points are located at the interface between two cells of the mesh, i.e. a point $x_{i+1/2}$ of the mesh is a transition point if $E_i \neq E_{i+1}$. The speed of propagation of the interface defines a discontinuity line $x = w t$ and let us introduce $\mathbf{U}^- = (A^-, Q^-)$ and $\mathbf{U}^+ = (A^+, Q^+)$ the (unknown) states respectively on the left hand side and on the right hand side of this line (see figure 6). The speed w is related to the unknowns \mathbf{U}^\pm by the Rankine-Hugoniot condition on the mass equation

$$\partial_t A + \partial_x Q = 0,$$

and thus w is given by:

$$w = \frac{Q^+ - Q^-}{A^+ - A^-}.$$

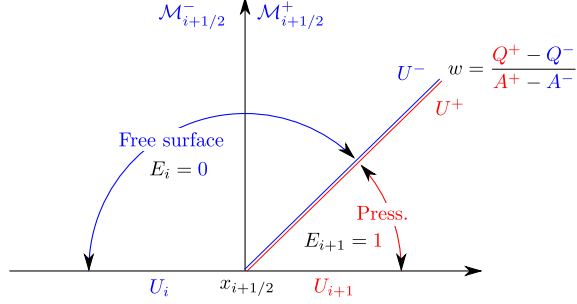


Figure 6: Rankine-Hugoniot condition through the line $x = wt$.
Free surface state propagating downstream.

According to the left U^- and right unknowns U^+ at the interface $x_{i+1/2}$ and the sign of the speed w , we have to deal with four cases:

- pressurized state propagating downstream,
- pressurized state propagating upstream,
- free surface state propagating downstream,
- free surface state propagating upstream.

Assume that U^\pm are given then the kinetic scheme in the case of transition points reads:

$$U_i^{n+1} = U_i^n + \frac{\Delta t^n}{h_i} (F_{i+\frac{1}{2}}^- - F_{i-\frac{1}{2}}^+)$$

where the numerical fluxes are computed by Equation (24) and the numerical microscopic interface quantities $\mathcal{M}_{i\pm 1/2}^{\pm, n}$ are obtained according to the formulas (22) and the sign of speed w as follows:

$$\mathcal{M}_{i+1/2}^- = \begin{cases} \mathcal{M}_{i+1/2}^-(\xi, \mathcal{M}_i^n, \mathcal{M}^-) & \text{if } w > 0, \\ \mathcal{M}_{i+1/2}^-(\xi, \mathcal{M}^+, \mathcal{M}_{i+1}^n) & \text{if } w < 0, \end{cases} \quad (27)$$

$$\mathcal{M}_{i+1/2}^+ = \begin{cases} \mathcal{M}_{i+1/2}^+(\xi, \mathcal{M}_i^n, \mathcal{M}^-) & \text{if } w > 0, \\ \mathcal{M}_{i+1/2}^+(\xi, \mathcal{M}^+, \mathcal{M}_{i+1}^n) & \text{if } w < 0. \end{cases}$$

where \mathcal{M}^\pm are the Gibbs equilibrium associated to U^\pm according to the formula (10).

A first way to compute the unknowns U^\pm called “the ghost waves approach” is to go back to the macroscopic level and to solve a linearized Riemann problem with discontinuous convection matrix.

The second way called “Full Kinetic Approach” computes the states \mathcal{M}^\pm at the microscopic level and the state U^\pm are recovered by the relations (12)-(13).

Only two of four cases are considered since we have two couples of “twin cases”: pressurized state is propagating downstream (or upstream) as shown in figure 7 and free surface state propagating downstream (or upstream) as shown in figure 8.

4.2.1 The ghost waves approach

In order to specify the unknowns U^\pm , we have to define four equations. To this end, the ghost waves approach is a way to obtain a system of four equations related to the **PFS** system. Adding the equations $\partial_t Z = 0$, $\partial_t \cos \theta = 0$ and $\partial_t S = 0$, the **PFS** model (without friction since it is taken into account in the term

\mathbf{Z} in the kinetic interpretation (15), (16)) can be written under a non-conservative form with the variable $\mathbf{V} = (Z, \cos \theta, S, A, Q)^t$:

$$\partial_t \mathbf{V} + D(\mathbf{V}) \partial_x \mathbf{V} = 0,$$

with D the convection matrix defined by

$$D(\mathbf{V}) = \begin{pmatrix} 0 & 0 & 0 & 0 & 0 \\ 0 & 0 & 0 & 0 & 0 \\ 0 & 0 & 0 & 0 & 0 \\ 0 & 0 & 0 & 0 & 1 \\ gA & gA\mathcal{H}(S_w) & \Psi(\mathbf{V}) & c^2(\mathbf{V}) - u^2 & 2u \end{pmatrix}$$

where $\Psi(\mathbf{V}) = gS\partial_S\mathcal{H}(S_w)\cos\theta - c^2(\mathbf{V})\frac{A}{S_w}$ and $u = Q/A$ denotes the speed of the water. $c(\mathbf{V})$ is then c for the pressurized flow or $\sqrt{g\frac{A}{T(A)}}\cos\theta$ for the free surface flow.

Remark 4.3. *Let us remark that, since $\partial_x I_1(x, A) = I_2(x, A) + \partial_A I_1(x, A)\partial_x A$, the pressure source term I_2 does not appear.*

We assume that the propagation of the interface (pressurized-free surface or free surface-pressurized) has a constant speed w during a time step. The ghost waves approach consists to solve a linearized Riemann problem in each zone (see [4]):

$$\begin{cases} \partial_t \mathbf{V} + \tilde{D} \partial_x \mathbf{V} & = 0, \\ \mathbf{V} & = \begin{cases} \mathbf{V}_l & \text{if } x < wt, \\ \mathbf{V}_r & \text{if } x > wt. \end{cases} \end{cases}$$

where $\tilde{D} = D(\tilde{\mathbf{V}})$. The term $\tilde{\mathbf{V}}$ is some approximation depending on the left \mathbf{V}_l and the right \mathbf{V}_r state.

The half line $x = wt$ is then the discontinuity line of \tilde{D} . Both states \mathbf{U}_i and \mathbf{U}^- (resp. \mathbf{U}_{i+1} and \mathbf{U}^+) correspond to the same type of flow. Thus it makes sense to define the averaged matrices in each zone as follows:

- for $x < wt$, we set $\tilde{D}_i = D(\tilde{\mathbf{V}}_i)$ for some approximation $\tilde{\mathbf{V}}_i$ which connects the state \mathbf{V}_i and \mathbf{V}^- .
- for $x > wt$, we set $\tilde{D}_{i+1} = D(\tilde{\mathbf{V}}_{i+1})$ for some approximation $\tilde{\mathbf{V}}_{i+1}$ which connects the state \mathbf{V}^+ and \mathbf{V}_{i+1} .

Then we formally solve two Riemann problems and use the Rankine-Hugoniot jump conditions through the line $x = wt$ which writes:

$$Q^+ - Q^- = w(A^+ - A^-), \quad (28)$$

$$F_2(A^+, Q^+) - F_2(A^-, Q^-) = w(Q^+ - Q^-), \quad (29)$$

with F_2 defined by (5). In what follows, all quantities of the form \tilde{v}_i (resp. \tilde{v}_{i+1}) define some approximation which connects the state v_i and v^- (resp. v^+ and v_{i+1}). States can be connected, for instance, by the mean value of each state.

Pressurized state propagating downstream: it is the case when on the left hand side of the line $\xi = wt$, we have a pressurized flow while on the right hand side we have a free surface flow and the speed w of the transition point is positive. Following Song [31] (see also [16]), an equivalent stationary hydraulic jump must occur from a supercritical to a subcritical condition and thus the characteristics speed satisfies the inequalities:

$$\tilde{u}_{i+1} + c(\tilde{\mathbf{V}})_{i+1} < w < \tilde{u}_i + c.$$

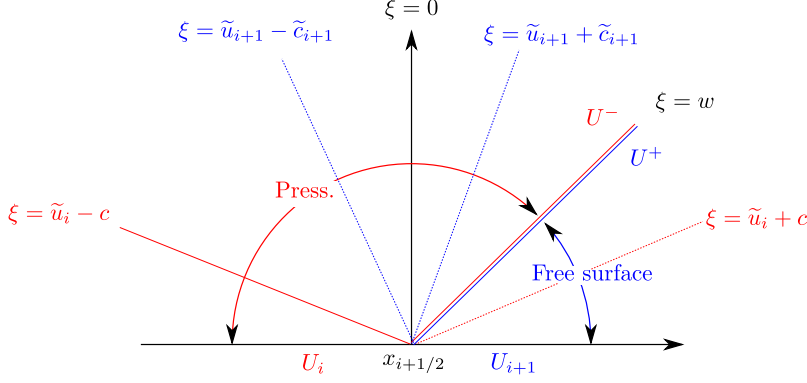


Figure 7: Pressurized state propagating downstream.

Therefore, only the characteristic lines drawn with solid lines are taken into account. Indeed they are related to incoming waves with respect to the corresponding space-time area $-\infty < \xi < w$. Conversely, the dotted line $\xi = \tilde{u}_{i+1} - c(\tilde{\mathbf{V}})_{i+1}$, for instance, related to the free surface zone but drawn in the area of pressurized flow is a “ghost wave” and is not considered. Thus $\mathbf{U}^+ = \mathbf{U}_{i+1}$ and $\mathbf{U}_i, \mathbf{U}^-$ are connected through the jumps across the characteristics $\xi = 0$ and $\xi = \tilde{u}_i - c$. Eliminating w in the Rankine-Hugoniot jump relations (28)-(29), we get \mathbf{U}^- as the solution to the nonlinear system:

$$\begin{aligned} (F_2(A_{i+1}, Q_{i+1}) - F_2(A^-, Q^-)) &= \frac{(Q_{i+1} - Q^-)^2}{(A_{i+1} - A^-)}, \\ Q^- - Q_i - (A^- - A_i)(\tilde{u}_i - c) + \frac{g\psi_i^{i+1}\tilde{A}_i}{c + \tilde{u}_i} &= 0, \end{aligned} \quad (30)$$

where ψ_i^{i+1} is the upwinded source term

$$\mathbf{Z}_{i+1} - \mathbf{Z}_i + \mathcal{H}(\tilde{S}_w)(\cos \theta_{i+1} - \cos \theta_i) + \Psi(\tilde{\mathbf{V}})(S_{i+1} - S_i).$$

Free surface state propagating downstream: it is the case when on the left hand side of the line $\xi = wt$, we have a free surface flow while on the right hand side we have a pressurized flow and the speed w of the transition point is positive. Following again Song [31], the characteristic speed satisfies the inequalities:

$$\tilde{u}_i + c(\tilde{\mathbf{V}})_i < w < \tilde{u}_{i+1} + c$$

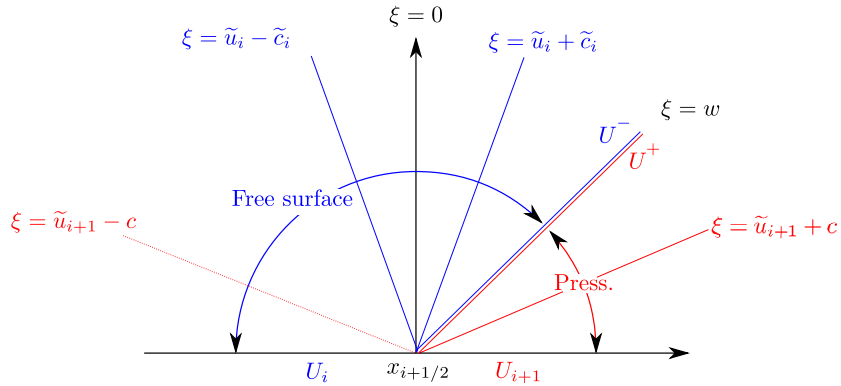


Figure 8: Free surface state propagating downstream.

There are two incoming characteristic lines with respect to the free surface area $-\infty < \xi < w$ (actually three with $\xi = 0$) and they can connect the given left state \mathbf{U}_i with any arbitrary free surface state. Thus only one characteristic line ($\xi = \tilde{u}_{i+1} + c$) gives any information (it is Equation (32) above) as an incoming characteristic line with respect to the pressurized zone $w < \xi < +\infty$. From the jump relations through the characteristic $\xi = 0$, and after the elimination of w in the Rankine-Hugoniot jump relations (28),(29) we get another equation, namely Equation (33) above. It remains to close the system of four unknowns (A^-, Q^-, A^+, Q^+). Thus, from Equation (6), we use the jump relation across the transition point (with speed w) for the total head $\Phi(A, Q, \cos \theta, \mathbf{Z}, E) = \frac{u^2}{2} + c^2 \ln \left(\frac{A}{S_w} \right) + g \mathcal{H}(A) \cos \theta + g \mathbf{Z}$, which writes:

$$\Phi^+ - \Phi^- = w(u^+ - u^-). \quad (31)$$

Finally, we use the relation:

$$w = w_{pred} \text{ with } w_{pred} = \frac{Q_{i+1} - Q_i}{A_{i+1} - A_i},$$

which is the predicted speed of the discontinuity. We have then to solve the nonlinear system:

$$(Q_{i+1} - Q^+) = (A_{i+1} - A^+) (\tilde{u}_{i+1} + c), \quad (32)$$

$$(Q^+ - Q^-) (Q_{i+1} - Q_i) = (A_{i+1} - A_i) (F_2(A^+, Q^+) - F_2(A^-, Q^-)), \quad (33)$$

$$\begin{aligned} \frac{(Q^+)^2}{2(A^+)^2} + c^2 \ln(A^+) + g \cos \theta \mathcal{H}(A^+) - \frac{(Q^-)^2}{2(A^-)^2} - c^2 \ln(A^-) - g \cos \theta \mathcal{H}(A^-), \\ = \frac{Q_{i+1} - Q_i}{A_{i+1} - A_i} \left(\frac{Q^+}{A^+} - \frac{Q^-}{A^-} \right), \end{aligned} \quad (34)$$

$$(Q_{i+1} - Q_i) (A^+ - A^-) = (Q^+ - Q^-) (A_{i+1} - A_i). \quad (35)$$

4.2.2 The Full Kinetic Approach

As we will show in the numerical experiments part of this article, the “ghost waves approach” method seems to produce very good results in agreement with experimental data. But, as we have shown in the previous section, to solve the interface problem between the free surface and the pressurized part of the flow, we have expressed mathematical relations between the macroscopic unknowns A and Q whereas in the free surface part as well as the pressurized part of the flow, we only deal with the microscopic quantities \mathcal{M}_i^n and we have constructed kinetic fluxes at the interface that take into account every source terms.

At this point, we proposed to solve the interface problem at the microscopic level. This method is based on the generalized characteristics method applied to the transport equation (15), see [13, 15].

As in the previous method, we will only consider two generic cases: pressurized state propagating downstream, as shown in figure 9(a), and free surface state propagating downstream, as shown in figure 9(b). For these two cases, we have to determine the Gibbs equilibrium \mathcal{M}^\pm corresponding to the macroscopic states \mathbf{U}^\pm on both sides of the curve Γ representing the trajectory of the transition point whose unknown velocity is w . On each time step, this trajectory is supposed to be a line and w must be defined such that the Rankine Hugoniot relations are satisfied.

We will now use the Gibbs equilibrium \mathcal{M}^- instead of \mathcal{M}_{i+1} in the computations of the microscopic fluxes, see formula (27), for the case $w > 0$

The transport equation (15) is used only for the transmission cases since we are only interested in trajectories which intersect Γ .

At the microscopic level, we obtain:

$$\forall \xi > w, \quad \mathcal{M}^-(\xi) \mathbb{1}_{\{|\xi|^2 + 2g \Delta \phi_{i+1/2}^n > 0\}} = \mathcal{M}_i^n \left(\sqrt{|\xi|^2 + 2g \Delta \phi_{i+1/2}^n} \right) \mathbb{1}_{\{|\xi|^2 + 2g \Delta \phi_{i+1/2}^n > 0\}},$$

and

$$\forall \xi < w, \quad \mathcal{M}^+(\xi) = \mathcal{M}_{i+1}^n(\xi).$$

These relations give, at the macroscopic level:

$$\int_w^{+\infty} \left(\frac{1}{\xi} \right) \mathcal{M}^-(\xi) \mathbb{1}_{\{|\xi|^2 + 2g \Delta \phi_{i+1/2}^n > 0\}} d\xi = \int_w^{+\infty} \left(\frac{1}{\xi} \right) \mathcal{M}_i^n \left(\sqrt{|\xi|^2 + 2g \phi_{i+1/2}^n} \right) \mathbb{1}_{\{|\xi|^2 + 2g \phi_{i+1/2}^n > 0\}} d\xi \quad (36)$$

and

$$\int_{-\infty}^w \left(\frac{1}{\xi} \right) \mathcal{M}^+(\xi) d\xi = \int_{-\infty}^w \left(\frac{1}{\xi} \right) \mathcal{M}_{i+1}^n(\xi) d\xi. \quad (37)$$

For the sake of simplicity, let us denote $c(A)$ the sound speed $b(x, A, E)$ defined by equation (11).

Let us mention that some preceding relations are obvious since the support of $\mathcal{M}(\xi)$ is $[u \pm c(A)\sqrt{3}]$. For instance for a free surface flow propagating downstream (or for the twin case of a pressurized flow propagating upstream), in the free surface zone, we have to compare in Equations (36) the velocity of the interface w with $u + c(A)\sqrt{3}$ while in the pressurized zone $u + c(A)\sqrt{3}$ is very large. The only corrective term is due to the slope.

From now on, we omit the indexes n to simplify the notations and every computations are done with the density function χ defined by (25).

Let us define the ‘‘effective’’ boundary in the integral used in Equations (36):

$$w' = \max \left(w, \sqrt{2g \max(0, -\phi_{i+1/2})} \right), \quad (38)$$

$$w'' = \max \left(\sqrt{\max(0, w^2 + 2g \Delta \phi_{i+1/2}^n)}, \sqrt{2g \max(0, \phi_{i+1/2})} \right). \quad (39)$$

Equations (36) write:

$$\frac{A^-}{c(A^-)} (\delta^- - \gamma^-) = \frac{A_i}{c(A_i)} \left(\sqrt{\delta_i^2 - 2g \phi_{i+1/2}} - \sqrt{\gamma_i^2 - 2g \phi_{i+1/2}} \right), \quad (40)$$

$$\frac{A^-}{c(A^-)} ((\delta^-)^2 - (\gamma^-)^2) = \frac{A_i}{c(A_i)} (\delta_i^2 - \gamma_i^2), \quad (41)$$

where $\gamma^-, \delta^-, \gamma_i, \delta_i$ are defined by:

$$\gamma^- = \max \left(w', u^- - c(A^-)\sqrt{3} \right), \quad \delta^- = \max \left(w', u^- + c(A^-)\sqrt{3} \right),$$

and

$$\gamma_i = \max \left(w'', u_i - c(A_i)\sqrt{3} \right), \quad \delta_i = \max \left(w'', u_i + c(A_i)\sqrt{3} \right).$$

In the same way, Equations (37) write:

$$\frac{A^+}{c(A^+)} (\beta^+ - \alpha^+) = \frac{A_{i+1}}{c(A_{i+1})} (\beta_{i+1} - \alpha_{i+1}), \quad (42)$$

$$\frac{A^+}{c(A^+)} ((\beta^+)^2 - (\alpha^+)^2) = \frac{A_{i+1}}{c(A_{i+1})} (\beta_{i+1}^2 - \alpha_{i+1}^2), \quad (43)$$

where $\alpha^+, \beta^+, \alpha_{i+1}, \beta_{i+1}$ are defined by:

$$\alpha^+ = \min \left(w, u^+ - c(A^+)\sqrt{3} \right), \quad \beta^+ = \min \left(w, u^+ + c(A^+)\sqrt{3} \right),$$

and

$$\alpha_{i+1} = \min \left(w, u_{i+1} - c(A_{i+1})\sqrt{3} \right), \quad \beta_{i+1} = \min \left(w, u_{i+1} + c(A_{i+1})\sqrt{3} \right).$$

Taking into account Equation (42), Equation (43) becomes:

$$\alpha^+ + \beta^+ = \alpha_{i+1} + \beta_{i+1}.$$

The unknowns are still w , A^- , Q^- , A^+ , Q^+ .

Pressurized state propagating downstream: let us first remark that in this case, since in the mesh i the flow is pressurized, we always have $w' \leq u_i + c(A_i)\sqrt{3}$ so that $\gamma^- - \delta^- \neq 0$. We solve then the system formed by the Rankine-Hugoniot jump conditions (28)-(29), and Equations (40), (41), and (42) which formed a full nonlinear system of 5 equations with 5 unknowns. So this procedure privileges the information coming from the zone containing the cell interface $x_{i+1/2}$.

Free surface state propagating downstream: again, we solve the nonlinear system formed by Equations (28)-(29), (40), (41) and (42) and the experience acquired with the industrial code FlowMix has shown that the system is a full nonlinear system of 5 equations with 5 unknowns.

But since in the mesh i the flow is a free surface one, we may have the critical case where $w' > u_i + c(A_i)\sqrt{3}$ with w' defined by Equation (38). In this case $\gamma^- - \delta^- = 0$ and the system formed by the nonlinear equations (28)-(29), (40), (41) and (42) is under determined. In this case, as in the ghost waves approach, we replace w by $w_{pred} = \frac{Q_{i+1} - Q_i}{A_{i+1} - A_i}$ and we solve the system formed by the Rankine-Hugoniot jump conditions (28), (29) and (31), as in the ghost waves approach, completed by Equations (42) and (43).

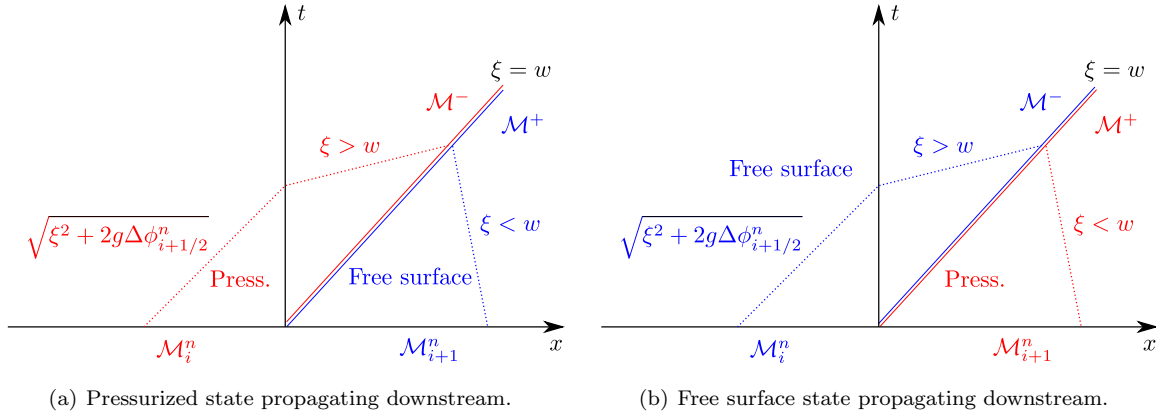


Figure 9: Full Kinetic Approach for the case of a transition point.

4.3 Boundary conditions

Let us recall that $x_{1/2}$ and $x_{N+1/2}$ are respectively the upstream and the downstream ends of the pipe. At this stage, we have computed all the “interior” states at time t^{n+1} , that is $(\mathbf{U}_i^{n+1})_{i=1,N}$ are computed, and also the state of the “interior” cells $(E_i^{n+1})_{i=1,N}$ by the method presented in section 4.4.

The upstream state \mathbf{U}_0 corresponds to the mean value of A and Q on the “fictitious” cell $m_0 = (x_{-1/2}, x_{1/2})$ (at the left of the upstream boundary of the pipe) and the downstream state \mathbf{U}_{N+1} corresponds to the mean value of A and Q on the “fictitious” cell $m_{N+1} = (x_{N+1/2}, x_{N+3/2})$ (at the right of the downstream end of the pipe).

Usually, we have to prescribe one boundary condition related to the state vectors \mathbf{U}_0^n and \mathbf{U}_{N+1}^n (there is generically only one incoming characteristics curve for the upstream and only one outgoing characteristics for the downstream). For instance, at the upstream end of the pipe, one of the following boundary conditions may be prescribed (we omit the index $n + 1$ for the sake of simplicity):

1. the water level is prescribed. So let $H_{up}(t)$ be a given function of time. Then we have:

$$\forall t > 0, \quad \frac{c^2}{g} \ln \left(\frac{A_0(t)}{S_{w0}(t)} \right) + \mathcal{H}(S_{w0}(t)) \cos \theta_0 + \mathbf{Z}_0 = H_{up}(t) . \quad (44)$$

2. the discharge is prescribed. So let $Q_{up}(t)$ be a given function of time. Then we have:

$$\forall t > 0, \quad Q_0(t) = Q_{up}(t) . \quad (45)$$

3. the total head may be prescribed. So let $\Phi_{up}(t)$ be a given function of time. Then we have:

$$\forall t > 0, \quad \frac{Q_0^2(t)}{2A_0(t)} + c^2 \ln \left(\frac{A_0(t)}{S_{w0}(t)} \right) + g\mathcal{H}(S_{w0}(t)) \cos \theta_0 + g\mathbf{Z}_0 = \Phi_{up}(t) . \quad (46)$$

At the downstream end, similar boundary conditions may be defined. In order to find a complete state for the upstream boundary, \mathbf{U}_0^{n+1} , and the downstream boundary, \mathbf{U}_{N+1}^{n+1} , we have to define the missing equation b_{up} and b_{down} respectively. We will present the method at the upstream boundary of the pipe (it is easy to adapt it at the downstream boundary).

At this stage, we have to consider two cases:

1. the upstream boundary is not a transition point, that is $E_0 = E_1$,
2. the upstream boundary is a transition point, that is $E_0 \neq E_1$.

We will treat the first case at the microscopic level while for the second case, we will describe the ‘‘Full Kinetic Approach’’ (the ‘‘ghost waves approach’’ for interior cells may be easily adapted).

4.3.1 The boundary is not a transition point

The jump $\Delta\phi_{1/2}^n$ is thus computed on the first half mesh.

Figure 10 represents the case when the upstream boundary of the pipe is not a transition point between free surface and pressurized flow. The Gibbs equilibrium \mathcal{M}_0 must be determined and we recall that we know either A_0 (if the upstream water level is prescribed by Equation (44)), Q_0 (if the upstream discharge is prescribed by Equation (45)) or a relation between these quantities (if the upstream total head is prescribed by Equation (46)).

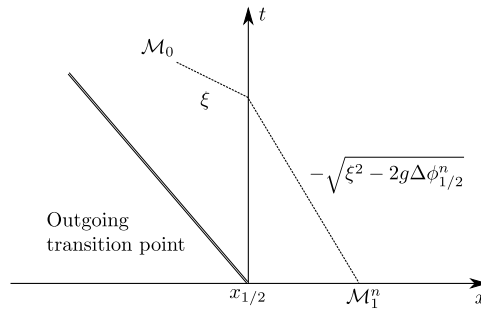


Figure 10: The upstream boundary of the pipe is not a transition point.

To obtain another equation denoted $b_{up}(A_0, Q_0)$, we will use the information transmitted from the outgoing kinetic characteristic (see figure 10). At the macroscopic level, we obtain:

$$\int_{-\infty}^{\xi_0} \begin{pmatrix} 1 \\ \xi \end{pmatrix} \mathcal{M}_0(\xi) d\xi = \int_{-\infty}^{\xi_0} \begin{pmatrix} 1 \\ \xi \end{pmatrix} \mathcal{M}_1^n \left(-\sqrt{|\xi|^2 - 2g \Delta \phi_{1/2}^n} \right) d\xi,$$

with $\xi_0 = -\sqrt{2g \max(0, \Delta \phi_{1/2}^n)}$. This also writes as:

$$\frac{A_0}{c(A_0)} (\delta_0 - \gamma_0) = \frac{A_1}{c(A_1)} \left(\sqrt{\gamma_1^2 + 2g \phi_{1/2}} - \sqrt{\delta_1^2 + 2g \phi_{1/2}} \right), \quad (47)$$

$$\frac{A_0}{c(A_0)} (\delta_0^2 - \gamma_0^2) = \frac{A_1}{c(A_1)} (\delta_1^2 - \gamma_1^2), \quad (48)$$

where $\gamma_0, \delta_0, \gamma_1, \delta_1$ are defined by:

$$\gamma_0 = \min \left(\xi_0, u_0 - c(A_0)\sqrt{3} \right), \quad \delta_0 = \min \left(\xi_0, u_0 + c(A_0)\sqrt{3} \right),$$

and

$$\gamma_1 = \min \left(\xi_1, u_1 - c(A_1)\sqrt{3} \right), \quad \delta_1 = \min \left(\xi_1, u_1 + c(A_1)\sqrt{3} \right),$$

and $\xi_1 = -\sqrt{2g \max(0, -\phi_{1/2}^n)}$.

So we will use only one of the two equations (47) or (48) as b_{up} .

Let us mention that in the case when $\gamma_1 = \delta_1$, Equations (47) and (48) are useless. This happens when:

- the flow is an incoming supcritical free surface flow at the upstream boundary condition (this could be due to a high slope inducing a great $|\xi_1|$). In this case, we impose the critical flow that is $u_0 = c(A_0)$.
- the flow is an outgoing supcritical free surface flow at the upstream boundary condition. The boundary conditions are then useless (two outgoing characteristics), so we impose $A_0 = A_1, Q_0 = Q_1$.

Remark 4.4. *We will use*

1. Equation (47) “momentum of order 0” if Q_0 is prescribed at the upstream end,
2. Equation (48) “momentum of order 1” if A_0 is prescribed at the upstream end,
3. Equation (48) if the total head is prescribed. Since Equation (46) couples the two unknowns, we had the choice between the two equations (47) and (48). The experience acquired with the industrial code `FlowMix` makes us to use Equation (48).

4.3.2 The boundary is a transition point

We suppose that $E_0 \neq E_1$. In the first step, we apply the procedure described in section 4.2.2: the left state is the downstream state \mathbf{U}_0 , known at time t^n , and the right state is \mathbf{U}_1 known at time t^{n+1} . We determine the state \mathbf{U}^- at the left of the transition curve. As the two states \mathbf{U}_0 and \mathbf{U}^- represent the same type of flow (free surface or pressurized), we apply the preceding method by just replacing \mathcal{M}_1^n by \mathcal{M}^- in all the formula above (see figure 11).

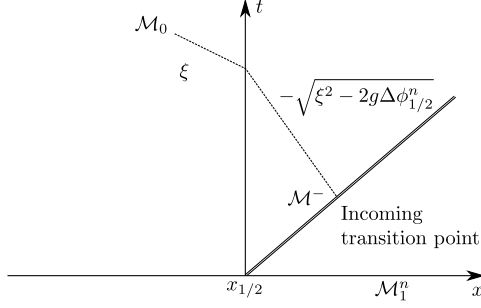


Figure 11: The upstream boundary of the pipe is a transition point.

4.4 Updating the state of the mesh E

To update the state of the mesh (see figure 12), we use a discrete version of the state indicator E equal to 1 for a pressurized flow and 0 otherwise. Following [8], after the computation of the wet area A_i^{n+1} , we predict the state of the cell m_i by the following criterion:

- if $E_i^n = 0$ then:
if $A_i^{n+1} < S_i$ then $E_i^{n+1} = 0$, else $E_i^{n+1} = 1$,
- if $E_i^n = 1$:
if $A_i^{n+1} \geq S_i$ then $E_i^{n+1} = 1$, else $E_i^n = E_{i-1}^n \cdot E_{i+1}^n$.

Indeed, if $A_i^{n+1} \geq S_i$ it is clear that the mesh m_i becomes pressurized, on the other hand if $A_i^{n+1} < S_i$ in a mesh previously pressurized, we do not know *a priori* if the new state is free surface ($\rho = \rho_0$ and the value of the wet area is less than S_i) or pressurized (in depression, with $\rho < \rho_0$ and the value of the wet area is equal to S_i : see Remark 4.5 and figure 13).

So far, as we do not take into account complex phenomena such as entrapment of air pockets or cavitation and keeping in mind that the CFL condition, defined by (26), ensures that a transition point crosses at most one mesh at each time step, we postulate that:

1. if the mesh m_i is free surface at time t^n , its state at time t^{n+1} is only determined by the value of A_i^{n+1} and it cannot become in depression.
2. if the mesh m_i is pressurized at time t^n and if $A_i^{n+1} < S_i$, it becomes free surface if and only if at least one adjacent mesh was free surface at time t^n . This is exactly the discrete version of the continuous $\frac{A}{S_w}$ criterion explained in Remark 4.5 and displayed on figure 13.

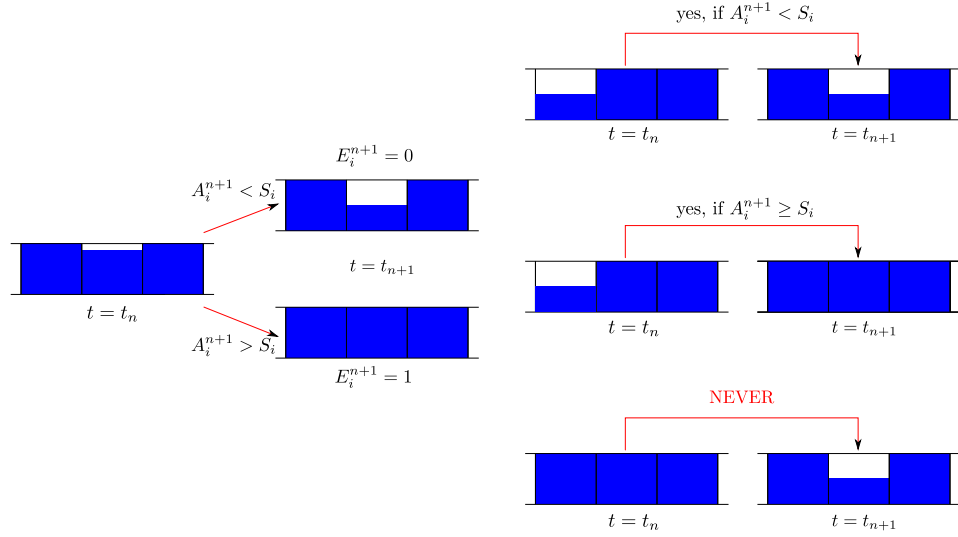


Figure 12: Update of the state E_i^{n+1} of the mesh m_i .

Remark 4.5. During a pressurized state, we may have $A > S$ or $A < S$. The case $A > S$ corresponds to an overpressure while the second one is observed for the depression. As said before, the main difficulty to detect depression comes from the fact that the criterion $A < S$ corresponds also to a free surface state. To dissociate these two cases, we have to know if $\rho = \rho_0$, that is also $\frac{A}{S_w} = 1$ or not. On figure 13, we represent how to detect a depression, overpressure and free surface state with the $\frac{A}{S_w}$ criterion. To this end, we show a physical situation at different time t_i , $i = 0, \dots, 3$. We draw the behavior of the interface speed w in the (x, t) -plane and the graph of the function $\frac{A}{S_w}$ at fixed time t_3 .

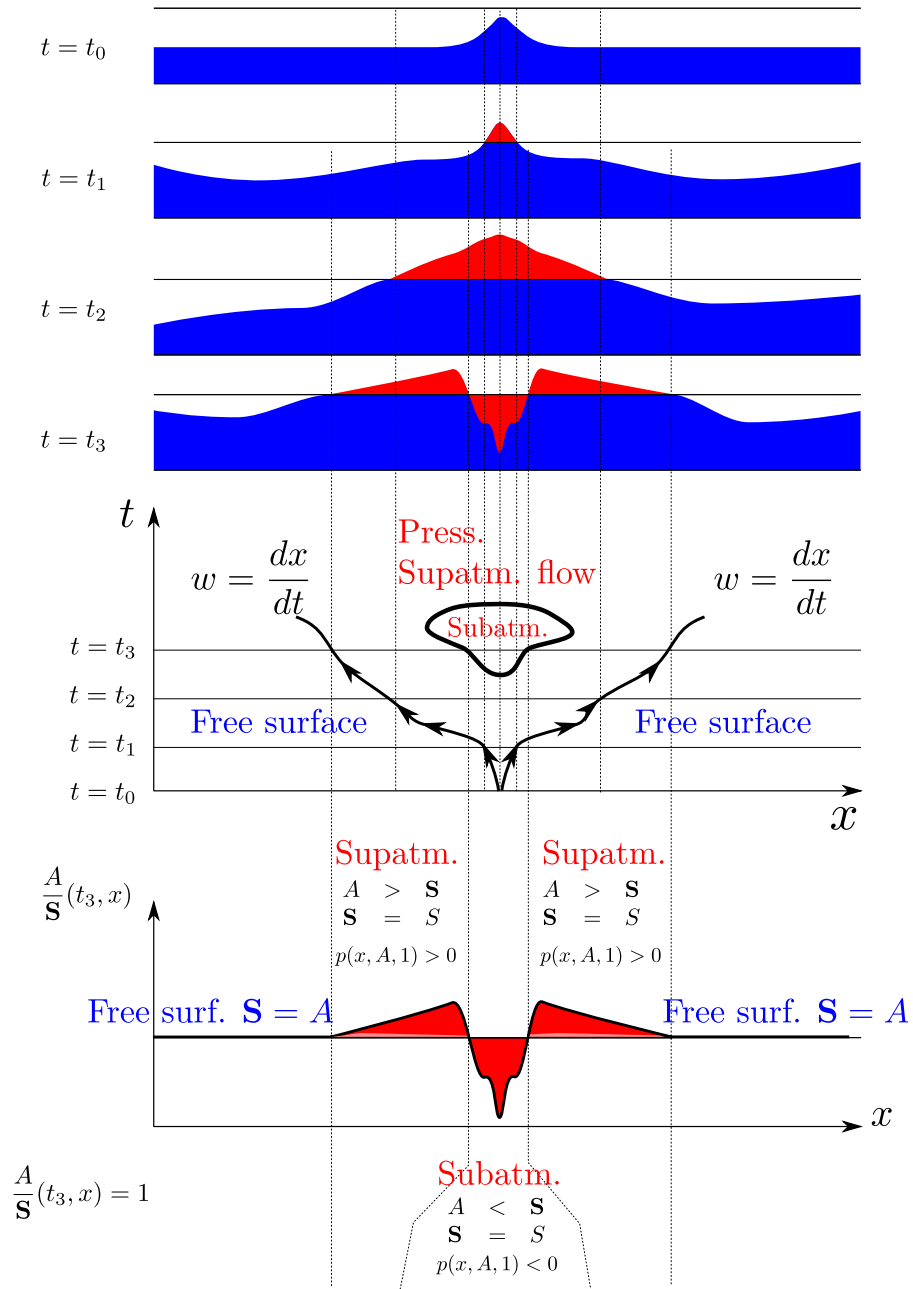


Figure 13: $\frac{A}{S_w}$ criterion to detect depression area.

5 Numerical experiments

This section is devoted to a numerical validation of the model and the kinetic numerical scheme for the following main cases:

- single point pressurized flow: the Wiggert's test case,

- a code to code validation for pressurized flow in uniform pipe,
- numerical computations of steady states: free surface steady state in non uniform pipe as well as “mixed” steady state in uniform pipe. We present a numerical study for the order of the discretisation.
- an example of drying and flooding flow,
- and finally a comparison between the two approaches : the ghost wave approach and the Full Kinetic Approach.

5.1 Single point pressurised flow

In this section, we present numerical results for the case of a single point pressurized flow, namely the test proposed by Wiggert [33]. The numerical results are then compared with the experimental ones: a very good agreement between them is shown. According to the experimental data, we were able to propose a value (or a range of values) for c which seems physically relevant. On the contrary, in the Preissmann slot technique ([33, 17]) the value of c is related to an arbitrary value (the width of the slot) and cannot exceed practically 10 m/s , otherwise the method becomes unstable. The following test case, is due to Wiggert [33]. The experimental device (see figure 14) is an horizontal 10 m long closed pipe with width 0.51 m and height $H = 0.148\text{ m}$. The Manning number is $1/K_s^2 = 0.012\text{ s/m}^{1/3}$. The initial conditions are a stationary state with the discharge $Q_0 = 0$ and the water level $h_0 = 0.128\text{ m}$.

Then a wave coming from the left side causes the closed channel to pressurise. The upstream condition is a given hydrograph (y_2 in figure 16), at the downstream end, a step function is imposed: the water level is kept constant to $h_0 = 0.128\text{ m}$ until the wave reaches the exit. At this time, the level is suddenly increased (see y_3 in figure 16). For the computations, these boundary conditions have been read on Wiggert’s article and rebuilt using piecewise polynomial interpolations (figure 15 below).

Other parameters are:

Discretisation points	: 80,
Delta x (m)	: 0.125,
CFL	: 0.5,
Simulation time (s)	: 18,
Sound speed (ms^{-1})	: 40.

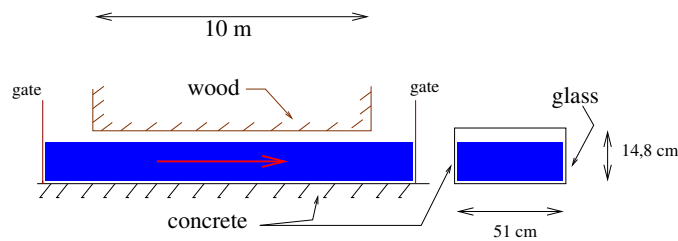


Figure 14: Experimental device (adapted from Wiggert [33]).

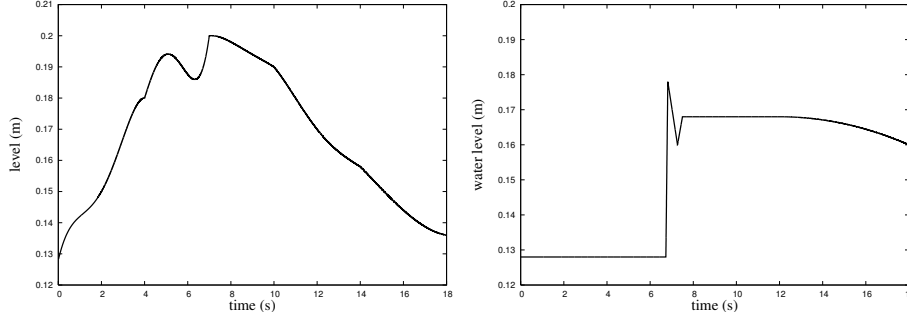


Figure 15: Wiggert's test : upstream hydrograph (up) and downstream water level (down).

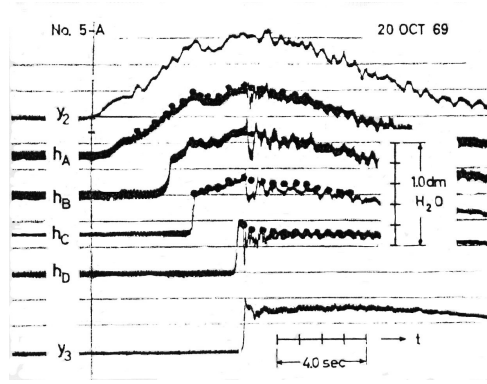


Figure 16: Wiggert : experimental data. y_2 : upstream hydrograph, y_3 : downstream hydrograph. h_A , h_B , h_C , h_D : pressure head at 0.5 m, 3.5 m, 5.5 m and 9.5 m from the tunnel entrance (location of recording instruments) ([33]).

Let us define the piezometric head by:

$$piezo = Z + \mathcal{H} + p \quad \text{with} \quad \begin{cases} p = \frac{c^2 (\rho - \rho_0)}{\rho_0 g} & \text{if the flow is pressurised,} \\ p = h & \text{the water height if the flow is free surface.} \end{cases}$$

In figure 17(a), we present the piezometric line computed at 3.5 m from the tunnel entrance (solid curve). Circles represent experimental data read on curve h_B , including maxima and minima points of the oscillating parts. We can observe a very good agreement with the experimental data even for the oscillating parts. We point out that we did not find in other papers, by authors carrying out the same simulation, a convenient numerical reproduction of these oscillations : they do not treat the dynamical aspect of the pressurized flow, in particular when using the Preissmann slot technique ([33, 17]). On the other hand, we found in M. Fuamba [16] a similar and interesting approach with a non conservative formulation and another numerical method (characteristics).

The value of the sound speed c was taken equal to 40 m/s, roughly according to the frequency of the oscillations observed during the phase of total submersion of the tunnel. This low value can be explained by the structure of the tunnel and by bubble flow (see [18, 32] for instance).

We observe that the front reaches the control point at 3.6 s, in a good agreement with the experimental data (less than 0.15 s late). Let us mention that before it reaches the exit (part AB in figure 17(a)) the oscillations of the pressure associated with the moving front reflect between upstream and the front itself (since the free surface is at constant pressure) where the channel is flooded. Beyond point B the oscillations

result from the step in the downstream water level and they propagate in the fully pressurized flow (their frequency was estimated using the BC part of the experimental curve).

Figure 17(b) gives the evolution of the front's speed. We observe the same behaviour as in [33, Figure 7]: the front quickly attains a maximum speed, decelerates and then slowly accelerates as it approaches the tunnel exit. Moreover the values are consistent with those of Wiggert.

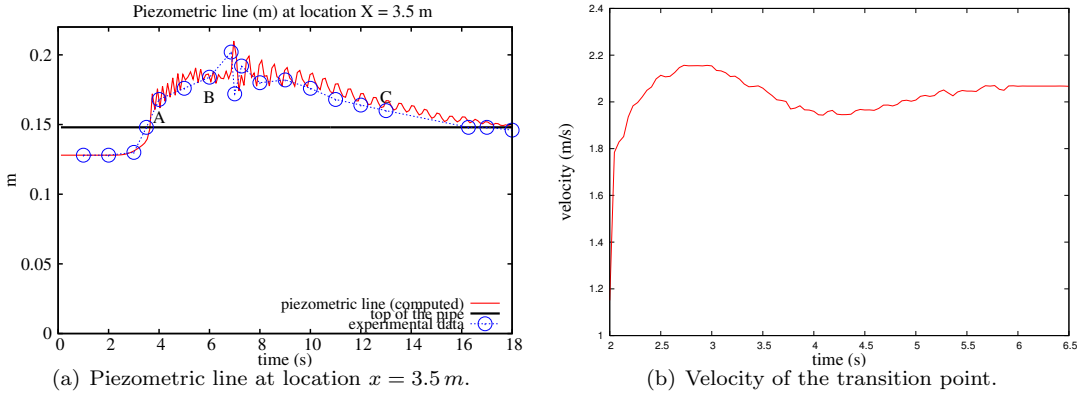


Figure 17: Numerical results for Wiggert's test.

5.2 Numerical validation for a pressurized flow in an uniform pipe

We present now numerical results of a water hammer test. The pipe of circular cross-section of 2 m^2 and thickness 20 cm is 2000 m long. The altitude of the upstream end of the pipe is 250 m and the angle is 5° . The Young modulus is $23 \cdot 10^9 \text{ Pa}$ since the pipe is supposed to be built in concrete: thus the sonic speed is equal to $c = 1414.2 \text{ m/s}$. The total upstream head is 300 m .

Other parameters are:

Discretisation points	: 1000,
Delta x (m)	: 2,
CFL	: 1,
Simulation time (s)	: 100,
Sound speed (ms^{-1})	: 1414.2.

To ensure that the model and the kinetic numerical method that we propose describe precisely flows in closed uniform water pipes, we present a validation of it by comparing numerical results of the proposed model with the ones obtained by solving Allievi equations by the method of characteristics with the so-called **belier** code used by the engineers of Electricité de France, Centre d'Ingénierie Hydraulique, Chambéry, [34].

A first simulation of the water hammer test is done for a fast cut-off of the downstream discharge for a pipe whose Strickler coefficient is $K_s = 90$: the initial downstream discharge is $10 \text{ m}^3/\text{s}$ and we cut the flow in 5 s . In figure 18, we present a comparison between the results obtained by our kinetic scheme and the ones obtained by the **belier** code at the middle of the pipe: the behavior of the piezometric line and the discharge at the middle of the pipe. One can observe that the results for the proposed model and the numerical kinetic scheme are in very good agreement with the solution of Allievi equations.

A second simulation of the water hammer test is done for the same rapid cut-off of the downstream discharge but for a frictionless pipe whose Strickler coefficient is $K_s = 215,63 \cdot 10^6$. In figure 19, we present a comparison between the results obtained by our kinetic scheme and the ones obtained by the **belier** code at the middle of the pipe: the behavior of the piezometric line and the discharge at the middle of the pipe. One can observe again that the results for the proposed model and the numerical kinetic scheme are in very good agreement with the solution of Allievi equations.

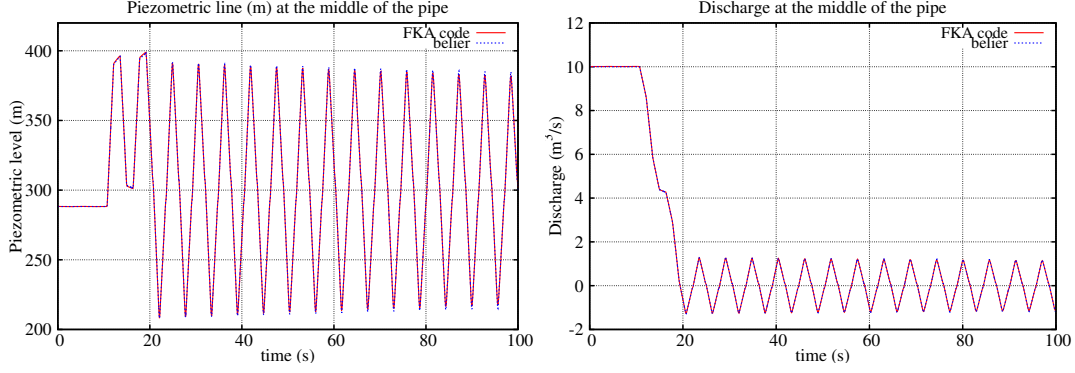


Figure 18: Piezometric line (left) and discharge (right) at middle of the pipe.

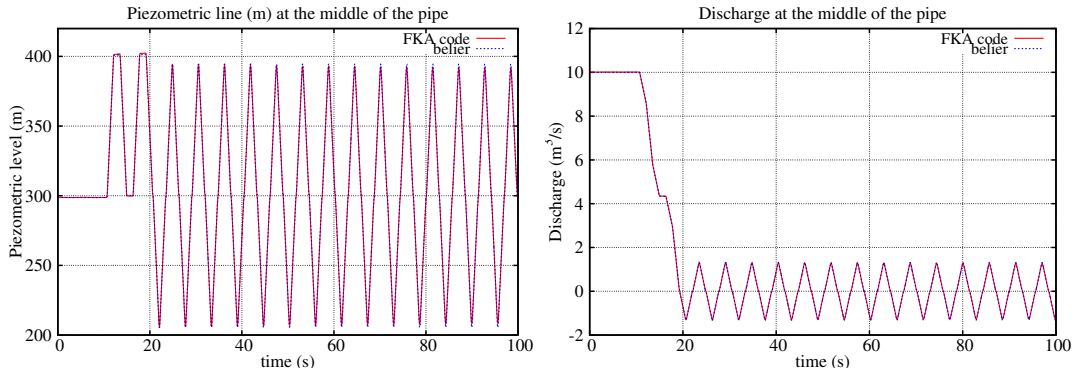


Figure 19: Piezometric line (left) and discharge (right) at middle of the frictionless pipe.

5.3 Numerical computation of steady states

5.3.1 Free surface steady state

Our purpose in the following test cases is to study the convergence in time and space towards a free surface steady state in a varying rectangular channel. We first test the ability of the presented scheme on two transcritical steady state test cases in a purely free surface flows for which analytic solutions are available. For each test case, the numerical spatial order is computed.

For all the free surface steady states, one has $\partial_t A = \partial_t u = \partial_t Q = 0$. Thus the mass-conservation equation gives $Q = Q_{ex} = Q_0$ and we get from Equation (6):

$$\partial_x Z = \partial_x \left(\mathcal{H}(A) \cos \theta + \frac{Q_0^2}{2gA^2} \right) + K(x, A) \frac{Q_0 |Q_0|}{A}.$$

Once the wet area A and the discharge are given, one can compute the corresponding topography. Thus, for instance, following MacDonald *et al.* [25] in case of varying rectangular channel with:

$$A(x) = B(x)h(x), \quad P(x, h) = B(x) + h,$$

the bed level Z is given by:

$$\partial_x Z = \left(\frac{Q_0^2}{gB(x)^2 h_{ex}(x)^3} - 1 \right) h'_{ex}(x) - \frac{Q_0^2 n^2 (2h_{ex}(x) + B(x))^{4/3}}{(B(x)h_{ex}(x))^{10/3}} + \frac{Q_0^2 B'(x)}{gB(x)^3 h_{ex}(x)^2},$$

where h_{ex} is the given height, B is the width of the channel, P is the wet perimeter and n is the Manning coefficient.

In this configuration, we reproduce two transcritical test cases with an hydraulic jump: the first one is subcritical to supercritical and the second is supercritical to subcritical. For each problem, we consider a channel of length $L = 1000\text{ m}$ of varying width

$$B(x) = 10 - 64 \left((x/L)^2 - 2(x/L)^3 + (x/L)^4 \right).$$

displayed on figure 20

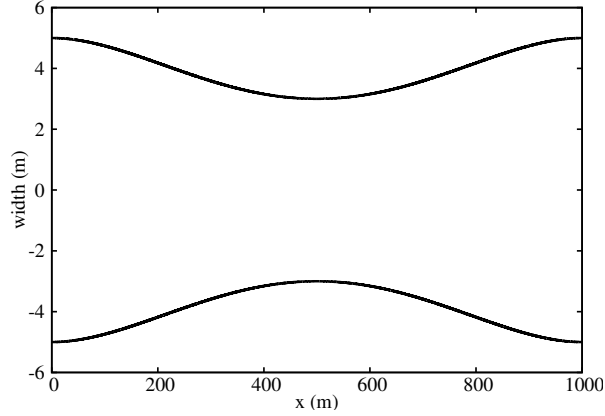


Figure 20: Width profile.

The discharge used for steady state is $Q_0 = 20\text{ m}^3/\text{s}$ and $n = 0.02$. The analytical solution is given by

$$h_{ex}(x) = \begin{cases} -1/40 + \frac{1}{1+2\left(\frac{2x-L}{2L}\right)^2} & \text{if } 0 \leq x \leq 500, \\ h_r(x) & \text{if } 500 < x \leq 1000, \end{cases} \quad (49)$$

where $h_r(x) = \sum_{i=1}^3 a_i \exp\left(-30i \frac{2x-L}{2L}\right) + a_4 \exp\left(\frac{4x-L}{4L}\right)$ is the solution on the right hand side of the hydraulic jump and the coefficients a_i are given following the test problem.

Remark 5.1. *As emphasized in [25], there is no analytical expression of Z . Therefore, we have constructed Z using cubic spline interpolation.*

Subcritical to supercritical test case .

In this test problem, the analytical solution is subcritical at inflow and changes, via a hydraulic jump localized at $x = 500\text{ m}$, to supercritical. The analytical solution is given by formula (49) where :

$$a_1 = 0.769035, a_2 = -0.755596, a_3 = 0.106813 \text{ and } a_4 = 1.125000 .$$

The analytical solution as well as the bed profil are shown in figure 21(a). The height at the upstream boundary is 0.641667 m and the height at downstream end is 1.125 m .

To compute the convergence of the numerical solution toward the steady state solution, the upstream total head is kept constant equal to 0.641667 m and the downstream water level to 1.125 m . Starting from a still water steady state with $h_{x=0} = 0.641667$, we compute the numerical flow for all time from $t = 0\text{ s}$ until the stationary state is reached. Then, the L^1 norm of the difference between (h, Q) computed by the

numerical kinetic scheme, for different mesh sizes of the uniform discretisation Δx , and the analytic solution (h_{ex}, Q_{ex}) at final time.

Other parameters are:

CFL	: 0.95,
Simulation time (s)	: 5000.
$\Delta x = L/N$: $N = (100 + m100)_{m=0,19}$ and 20000.

We present, in figure 21, the piezometric line (see figure 21(a)) and the discharge (see figure 21(c)) of the flow along the pipe when the steady state is reached for four different mesh sizes $\Delta x = 10$, $\Delta x = 5$, $\Delta x = 1$ and $\Delta x = 0.05$. In figure 21(a) and 21(b), the four curves representing the piezometric line, compared to the analytical one, are close to the analytical solution and the hydraulic jump location are very well captured even if, for large Δx , the numerical solution is smooth around this point. For the discharge, we observe that the convergence toward $Q_0 = 20 \text{ m}^3/\text{s}$ is also close, since for $\Delta x = 100$, the error is of order 0.1 and decreases as Δx . Indeed, in figure 21(d), we have computed the L^1 norm. The obtained numerical order is almost equal to 1 in h as well as for Q .

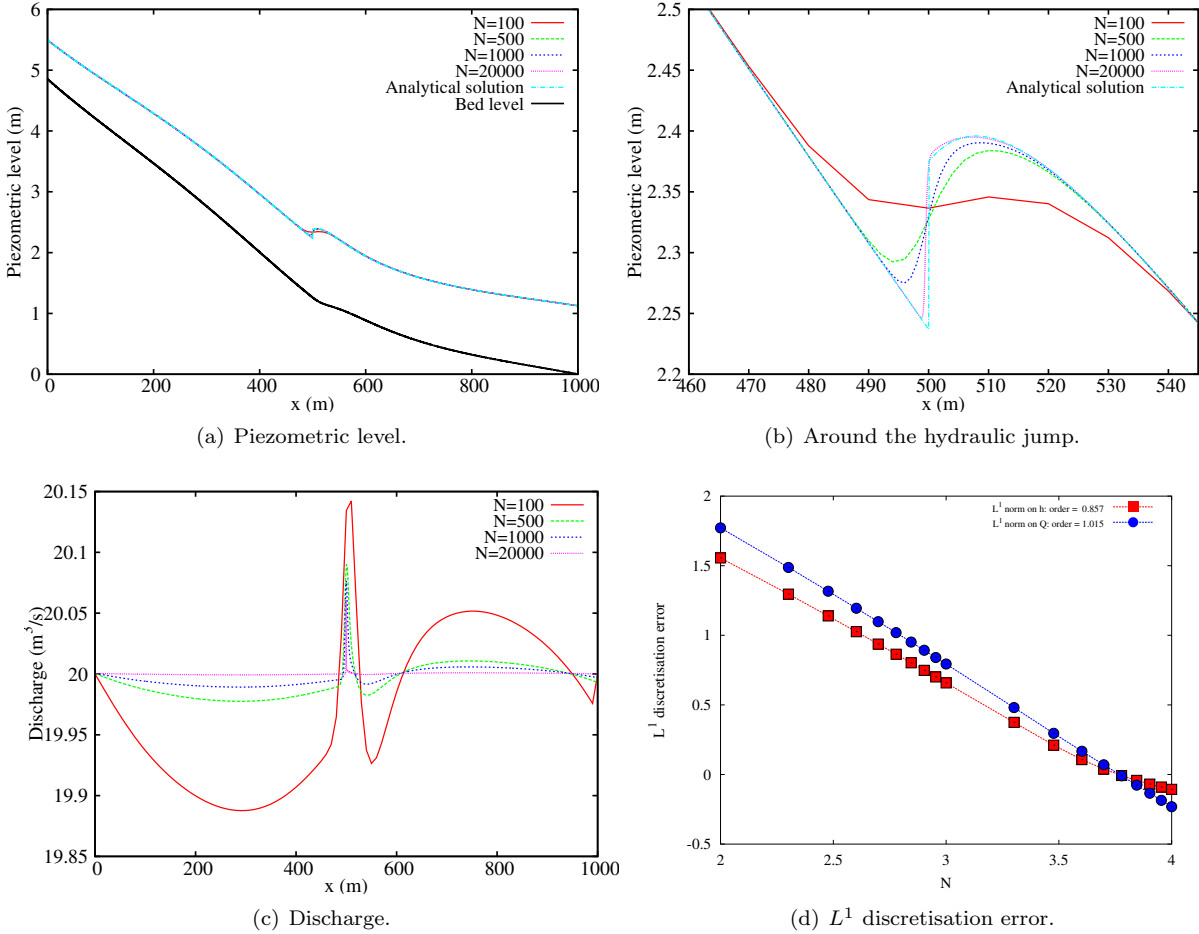


Figure 21: Subcritical to supercritical test case.

Supercritical to subcritical test case.

In this test problem, the analytical solution is supercritical at inflow and changes, via a hydraulic jump

localized at $x = 500 \text{ m}$, to subcritical. The analytical solution here is given by formula (49) where

$$a_1 = -0.230680, a_2 = 0.248267, a_3 = -0.228271 \text{ and } a_4 = 1.500000 .$$

The analytical solution as well as the bed profile are shown in figure 22(a). The height at the upstream boundary is 0.641667 m and the height at downstream end is 1.5 m .

We proceed as done before to compute the convergence of the numerical solution toward the steady state. Results on the piezometric line, the discharge and the numerical order are displayed on figure 22. We have used the same parameters as in the previous section. As one can observe, the same conclusion holds.

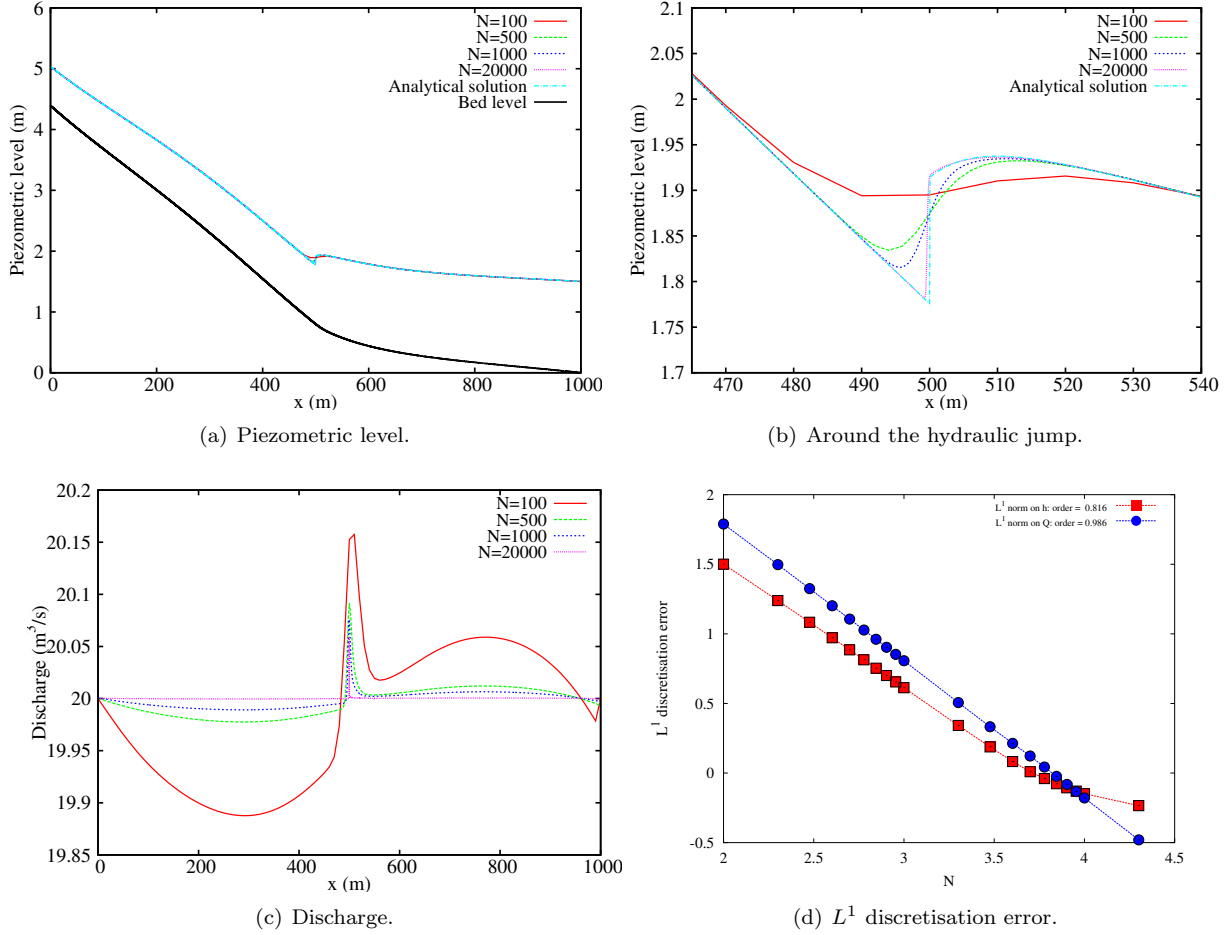


Figure 22: Supercritical to subcritical test case.

5.3.2 Mixed steady state

In order to obtain a qualitative behavior of the scheme and to compute a “numerical” order of the discretisation error of the kinetic numerical scheme, we present now a numerical experiment where the steady state is mixed. The pipe is a circular pipe of diameter 3 m and 100 m long with slope 0.001 and Strickler coefficient is $K_s = 63.7$. The altitude of the upstream end of the pipe is 100 m . The upstream total head is kept constant equal to 104 m whereas the downstream water level varies (see figure 23). We have computed the “exact” numerical flow for all time from $t = 0 \text{ s}$ until the stationary state is reached at time $t = 100 \text{ s}$, by the VFRoe method presented in [4] with a uniform discretisation of 8000 mesh points. We have then computed

the L^1 norm of the difference between the piezometric line computed by the numerical kinetic scheme for different mesh sizes of the uniform discretisation, Δx , and the “exact” numerical solution at time $t = 20$ s and $t = 100$ s.

Other parameters are:

CFL	:	0.9,
Simulation time (s)	:	100,
Sound speed (ms^{-1})	:	40.

We present, in figure 24, the piezometric line and the speed of the flow along the pipe at time $t = 20$ s for three different mesh sizes (in fact we prefer to talk of the number of mesh points). The three curves representing the piezometric line are very close *whereas* the coarse mesh does not capture at all the speed along the pipe.

We present, in figure 25, the piezometric line and the speed of the flow along the pipe at time $t = 100$ s. The three curves representing the piezometric line *as well as* the speed along the pipe are very close. One can see that the stationary speed is not constant along the pipe.

The numerical order at time $t = 20$ s, represented in figure 26(a) for different mesh sizes, and the numerical order at time $t = 100$ s, represented in figure 26(b), are almost equal to 1, which was expected since a kinetic finite volume scheme is known to be of order 1.

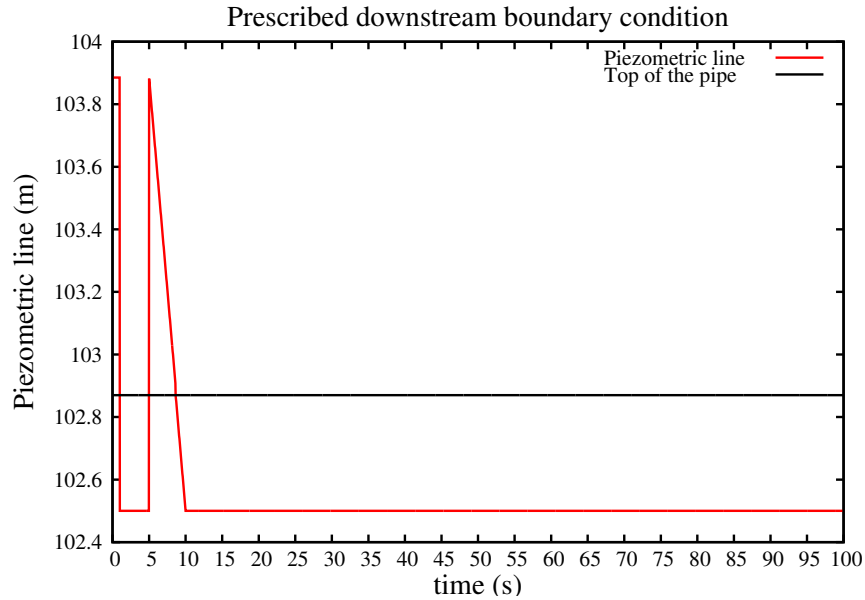
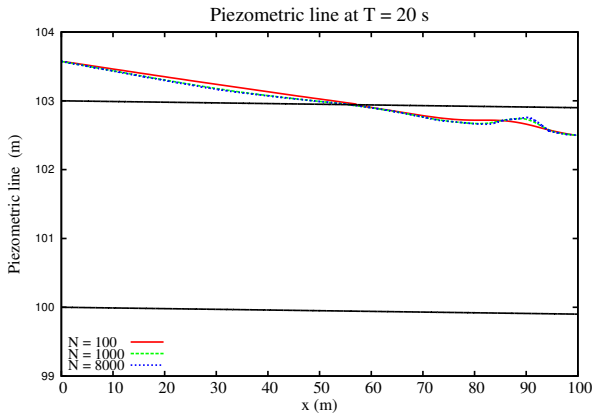
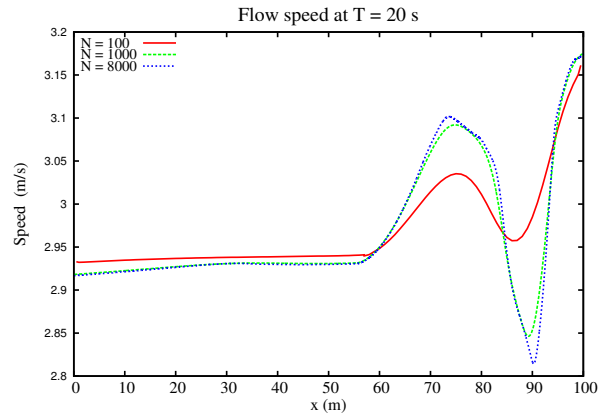


Figure 23: Piezometric line at the downstream end of the pipe.

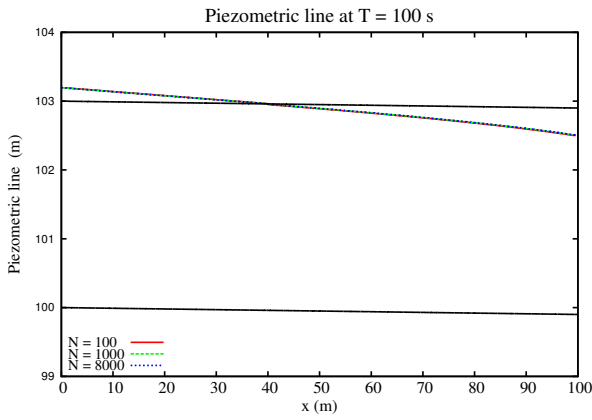


(a) Piezometric line.

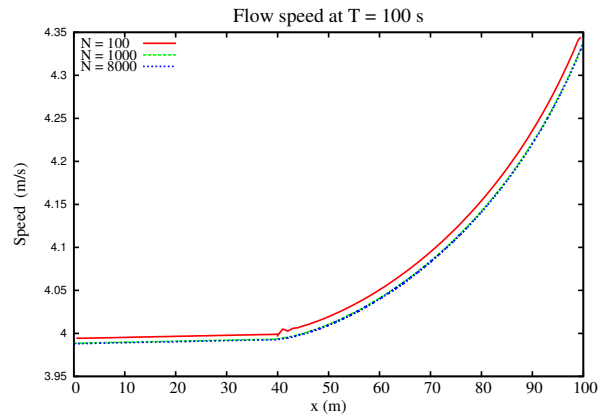


(b) Speed along the pipe.

Figure 24: Piezometric line and speed along the pipe at time $t = 20$ s.



(a) Piezometric line.



(b) Speed along the pipe.

Figure 25: Piezometric line and speed along the pipe at time $t = 100$ s.

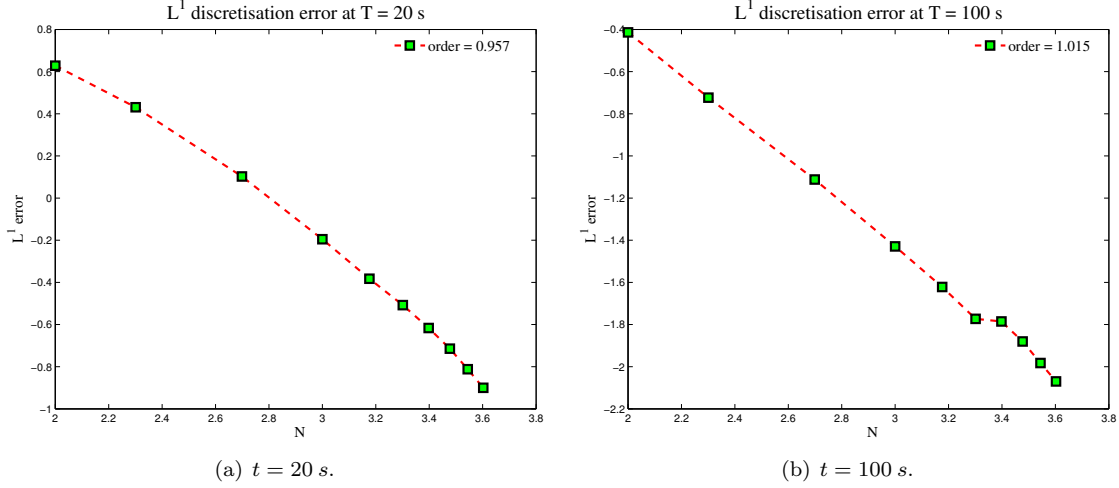


Figure 26: L^1 discretisation error versus N in 10-logarithmic scale at time $t = 20$ s and time $t = 100$ s.

Finally, although we do not know if the two numerical schemes that we proposed satisfy the conservative in cell entropy (see Equation (8)), every numerical results presented have a very good qualitative behavior.

5.4 Numerical validation for drying and flooding flow

We present now numerical results for a flow that will be drying and flooding. The frictionless pipe is constituted by a pipe of circular cross-section of diameter 2 m and 50 m long with slope 0.003 and another pipe of circular cross-section of diameter 2 m and 100 m long with slope 0.05 . The altitude of the upstream end of the pipe is 100 m. The upstream and downstream discharge is kept to 0 .

Other parameters are:

First pipe discretisation points	: 100,
Delta x (m)	: 0.5,
Second pipe discretisation points	: 200,
Delta x (m)	: 0.5,
CFL	: 0.9,
Simulation time (s)	: 500,
Sound speed (ms^{-1})	: 10.

The initial state is a flow of constant height (1.8 m) on half the first pipe and a dry zone on the rest of the pipe, see figure 27. We present the flow at time $T = 6$ s, see figure 28, where a drying zone is present, at time $T = 80$ s, see figure 29, when the flow has reached the downstream end and is partially pressurized and the flow at the final time $T = 500$ s, see figure 30 where all the water is in the second pipe. This non physical test shows that the kinetic numerical scheme treats “naturally” the flooding zone and almost the drying zone (up the rounding error of the computer). The water height is exactly equal to 0 , in the initial condition and at the final time for the dry zones.

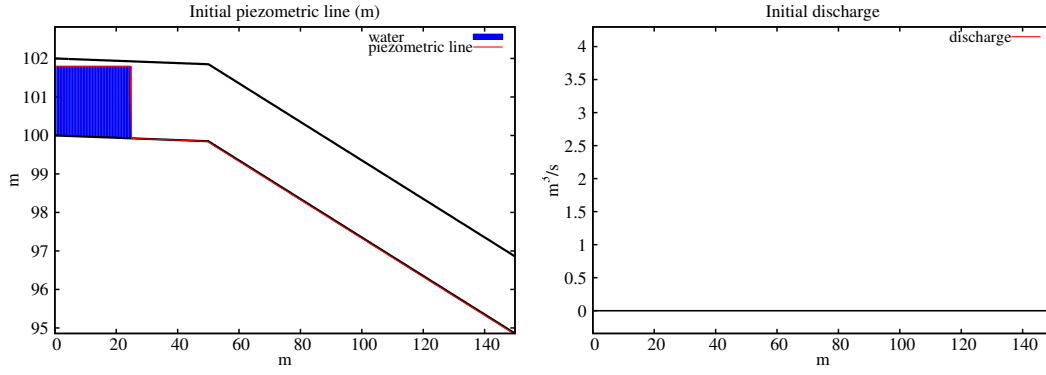


Figure 27: Piezometric line (left) and discharge (right) at initial condition.

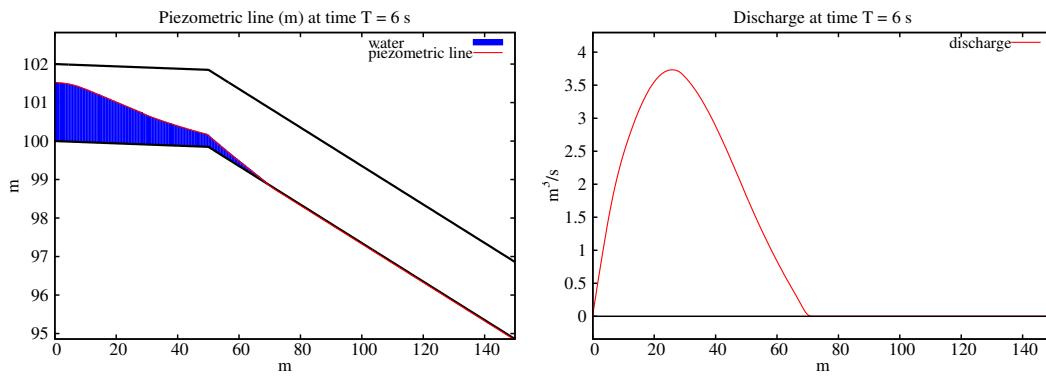


Figure 28: Piezometric line (left) and discharge (right) at time $T = 6$ s.

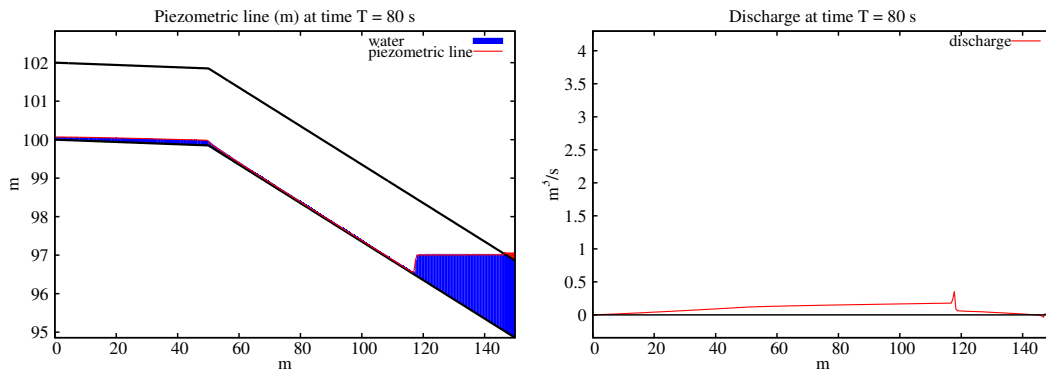


Figure 29: Piezometric line (left) and discharge (right) at time $T = 80$ s.

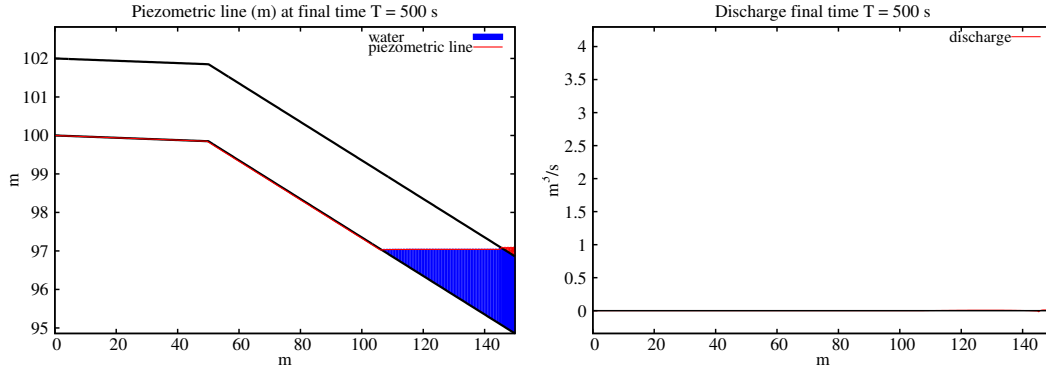


Figure 30: Piezometric line (left) and discharge (right) at final time $T = 500$ s.

5.5 “Ghost waves approach” versus “Full Kinetic Approach”

We want to compare numerically the two approaches on a violent water hammer “numerical” test for a non uniform frictionless closed water pipes.

To this end, the numerical experiment is performed in the case of an expanding 5 m long closed circular water pipe with 0 slope. The upstream diameter is 2 m and the downstream diameter is 3.2 m. The altitude of the main pipe axis is set to $Z = 1$ m.

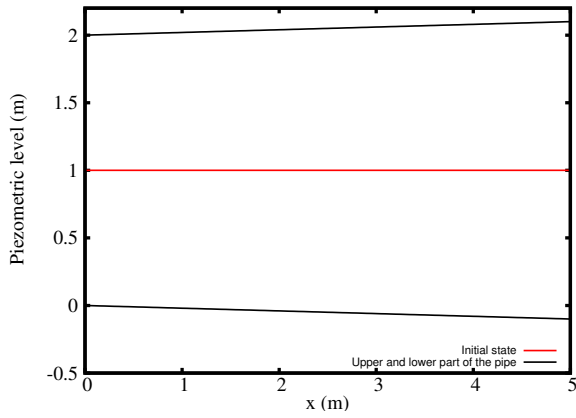
At the upstream boundary condition, the piezometric line (increasing linearly from 1 m to 3.2 m in 5 s) is prescribed while the downstream discharge is kept constant equal to $0 \text{ m}^3/\text{s}$ (see figure 31). The simulation starts from a still water free surface steady state where the height of the upstream is 1 m (see figure 31) and the discharge is null.

Other parameters are

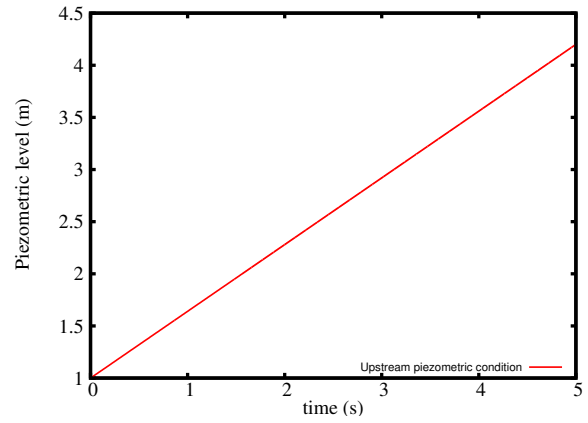
Discretisation points	: 100,
Delta x (m)	: 0.05,
CFL	: 0.8,
Simulation time (s)	: 5,
Sound speed (m s^{-1})	: 20.

Let us mention that we have already used this numerical test case to compare the kinetic scheme using the “ghost waves approach” with the VFRoe scheme presented in [4], see [5, Figure 3].

This numerical test intends to reproduce a “sharp” water hammer experiment inducing large oscillations of the piezometric level and the discharge as showed in figures 32 and 33. From a numerical point of view, it is a “hard” numerical test. In order to validate numerically this approach and due to the lack of experimental data in the case of variable cross section pipes, we compare the result of the presented numerical scheme with those obtained by the upwinded VFRoe scheme [4]. Results are represented in figures 32 and 33 where we have plotted the piezometric line, especially the transition point at different times $t = 1.6$ s, $t = 1.7$ s, $t = 1.8$ s, $t = 1.9$ s. In figures 32 and 33, the left side to the transition point corresponds to a free surface state and the right one to a pressurized except at $t = 1.9$ s where we can observe two transition points due to the pressurized state propagating from the downstream end. The behavior of the two methods are in a good agreement and particularly with respect to the localization of transition points. This short and “sharp” water hammer test allows us to validate numerically the two approaches for capturing the transition between free surface and pressurized flow.

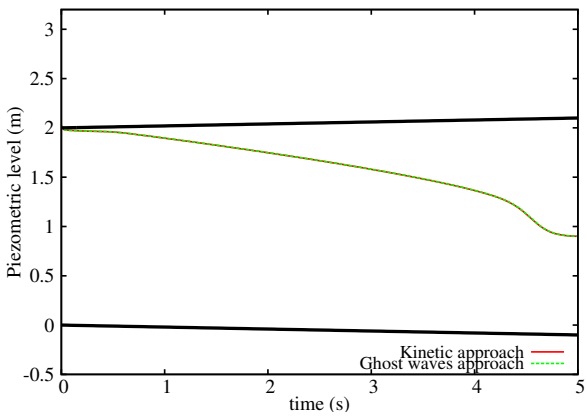


(a) Initial state.

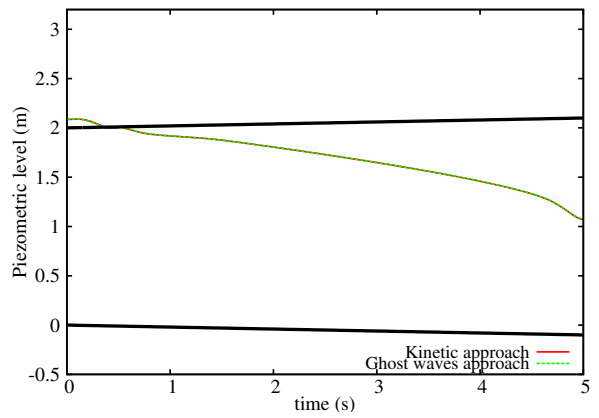


(b) Prescribed upstream boundary condition.

Figure 31: Initial state and boundary conditions.



(a) $t = 1.6$ s.



(b) $t = 1.7$ s.

Figure 32: Water hammer test case in non uniform closed water pipe.

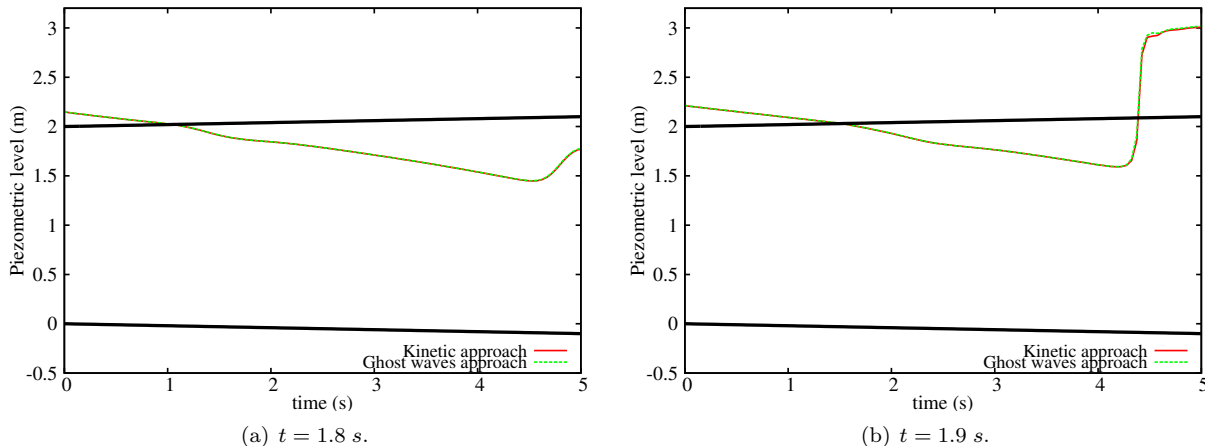


Figure 33: Water hammer test case in non uniform closed water pipe.

6 Conclusion and perspectives

We have proposed in this work a new manner to extend the numerical kinetic scheme with reflections build by Perthame and Simeoni [29], to closed water pipes with varying sections and not only to rectangular closed water pipes. This scheme is wet area conservative and under a CFL condition preserves the positivity of the wet area.

As a well known feature of general kinetic schemes, we are able to “naturally” deal with flows where a flooding zone may be present. This key property was not solved by the previous VFRoe scheme that we proposed in [4] without introducing a cut-off function for the wetted area which may causes a loss of conservativity.

The **PFS** model is numerically solved by a kinetic scheme with reflections using the interfacial upwind of all the source terms into the numerical fluxes.

As mentioned in [8, 4] this numerical method reproduces correctly laboratory tests for uniform pipes (Wiggert’s test case) and can deal with multiple transition points between the two types of flows. The code to code comparison for pressurized flows in uniform pipes has proved the robustness of the method. But due to the lack of experimental data for drying and flooding flows, we have only shown the behavior of the piezometric line which seems reasonable (at less no major difference was observed). For non uniform pipes, the two numerical schemes are in a very good agreement even though we are not in possession of experimental data.

We are at the present time interested in the construction of a class of “in cell entropy satisfying” schemes consistent with the numerical approximations of hyperbolic systems with source terms.

The next step is to take into account the air entrainment which may have non negligible effects on the behavior of the piezometric head. A first approach has been derived in the case of perfect fluid and perfect gas modeled s a bilayer model based on the **PFS** model [7].

Acknowledgements

This work is supported by the “Agence Nationale de la Recherche” referenced by ANR-08-BLAN-0301-01 and the second author was supported by the ERC Advanced Grant FP7-246775 NUMERIWAVES. This work was finalized while the third author was visiting BCAM–Basque Center for Applied Mathematics, Derio, Spain, and partially supported by the ERC Advanced Grant FP7-246775 NUMERIWAVES. The third author wishes to thank Enrique Zuazua for his kind hospitality.

Moreover, the authors wish to thank the referees for their remarks and the careful reading of the numerical scheme presented in this paper.

References

- [1] F. BOUCHUT, *Nonlinear stability of finite volume methods for hyperbolic conservation laws and well-balanced schemes for sources*, Birkhäuser, 2004.
- [2] F. BOUCHUT AND M. WESTDICKENBERG, *Gravity driven shallow water models for arbitrary topography*, Commun. Math. Sci., 2 (2004), pp. 359–389.
- [3] C. BOURDARIAS, M. ERSOY, AND S. GERBI, *A kinetic scheme for pressurised flows in non uniform closed water pipes*, Monografias de la Real Academia de Ciencias de Zaragoza, 31 (2009), pp. 1–20.
- [4] C. BOURDARIAS, M. ERSOY, AND S. GERBI, *A model for unsteady mixed flows in non uniform closed water pipes and a well-balanced finite volume scheme*, Int. J. Finite Vol., 6 (2009), pp. 1–47.
- [5] C. BOURDARIAS, M. ERSOY, AND S. GERBI, *A kinetic scheme for transient mixed flows in non uniform closed pipes: a global manner to upwind all the source terms*, Journal of Scientific Computing, 48 (2011), pp. 89–104.
- [6] ———, *A mathematical model for unsteady mixed flows in closed water pipes*, Science China Mathematics, 55 (2012), pp. 221–244.
- [7] ———, *Air entrainment in transient flows in closed water pipes: a two-layer approach*, ESAIM M2AN, Math. Model. Numer. Anal., 47 (2013), pp. 507–538.
- [8] C. BOURDARIAS AND S. GERBI, *A finite volume scheme for a model coupling free surface and pressurised flows in pipes*, J. Comp. Appl. Math., 209 (2007), pp. 109–131.
- [9] ———, *A conservative model for unsteady flows in deformable closed pipe and its implicit second order finite volume discretisation*, Computers & Fluids, 37 (2008), pp. 1225–1237.
- [10] ———, *A kinetic scheme for unsteady pressurised flows in closed water pipes*, J. Comp. Appl. Math., 234 (2010), pp. 2098–2105.
- [11] C. BOURDARIAS, S. GERBI, AND M. GISCLON, *A kinetic formulation for a model coupling free surface and pressurised flows in closed pipes*, J. Comp. Appl. Math., 218 (2008), pp. 522–531.
- [12] H. CAPART, X. SILLEN, AND Y. ZECH, *Numerical and experimental water transients in sewer pipes*, Journal of Hydraulic Research, 35 (1997), pp. 659–672.
- [13] C. M. DAFERMOS, *Generalized characteristics in hyperbolic systems of conservation laws*, Arch. Rational Mech. Anal., 107 (1989), pp. 127–155.
- [14] N. T. DONG, *Sur une méthode numérique de calcul des écoulements non permanents soit à surface libre, soit en charge, soit partiellement à surface libre et partiellement en charge*, La Houille Blanche, 2 (1990), pp. 149–158.
- [15] M. ERSOY, *Modélisation, analyse mathématique et numérique de divers écoulements compressibles ou incompressibles en couche mince*, PhD thesis, Université de Savoie, 2010. available at <http://tel.archives-ouvertes.fr/tel-00529392>.
- [16] M. FUAMBA, *Contribution on transient flow modelling in storm sewers*, Journal of Hydraulic Research, 40 (2002), pp. 685–693.

- [17] P. GARCIA-NAVARRO, F. ALCRUDO, AND A. PRIESTLEY, *An implicit method for water flow modelling in channels and pipes*, Journal of Hydraulic Research, 32 (1994), pp. 721–742.
- [18] M. HAMAM AND A. MCCORQUODALE, *Transient conditions in the transition from gravity to surcharged sewer flow*, Can. J. Civ. Eng., 9 (1982), pp. 189–196.
- [19] F. KERGER, P. ARCHAMBEAU, S. ERPICUM, B. J. DEWALS, AND M. PIROTON, *Numerical simulation of highly transient mixed flow in sewer system*, La Houille Blanche, 5 (2009), pp. 159–167.
- [20] ———, *Exact Riemann solver and Godunov scheme for simulating highly transient mixed flows*, J. Comp. Appl. Math., 235 (2011), pp. 2030–2040.
- [21] ———, *A fast universal solver for 1D continuous and discontinuous steady flows in rivers and pipes*, Int. J. for Num. Meth. in Fluids., 6 (2011), pp. 33–43.
- [22] D. KRÖNER, P. LEFLOCH, AND M. THANH, *The minimum entropy principle for compressible fluid flows in a nozzle with discontinuous cross-section*, ESAIM M2AN, Math. Model. Numer. Anal., 42 (2008), pp. 425–442.
- [23] D. KRÖNER AND M. THANH, *Numerical solutions to compressible flows in a nozzle with variable cross-section*, SIAM J. Numer. Anal., 43 (2005), pp. 796–824.
- [24] P. LEFLOCH AND M. THANH, *A godunov-type method for the shallow water equations with discontinuous topography in the resonant regime*, J. Comput. Physics, 230 (2001), pp. 7631–7660.
- [25] I. MACDONALD, M. J. BAINES, N. K. NICHOLS, AND P. G. SAMUELS, *Comparison of some steady state Saint-Venant solvers for some test problems with analytic solutions*, Tech. Rep. Numerical Analysis Report 2/95, Department of Mathematics, University of Reading, UK, 1995.
- [26] A. MANGENY, F. BOUCHUT, N. THOMAS, J. P. VILOTTE, AND M. O. BRISTEAU, *Numerical modeling of self-channeling granular flows and of their level-channel deposits*, J. of Geophys. Res., 112 (2007), pp. 1–21.
- [27] G. D. MASO, P. G. LEFLOCH, AND F. MURAT., *Definition and weak stability of nonconservative products*, J. Math. Pures Appl., 74 (1995), pp. 483–548.
- [28] B. PERTHAME, *Kinetic formulation of conservation laws*, vol. 21 of Oxford Lecture Series in Mathematics and its Applications, Oxford University Press, Oxford, 2002.
- [29] B. PERTHAME AND C. SIMEONI, *A kinetic scheme for the Saint-Venant system with a source term*, Calcolo, 38 (2001), pp. 201–231.
- [30] P. ROE, *Some contributions to the modelling of discontinuous flow*, in Large-scale computations in fluid mechanics. Part 2. Proceedings of the fifteenth AMS-SIAM summer seminar on applied mathematics held at Scripps Institution of Oceanography, La Jolla, Calif., June 27-July 8, 1983, B. E. Engquist, S. Osher, and R. C. J. Somerville, eds., vol. 22 of Lectures in Applied Mathematics, American Mathematical Society, 1985, pp. 163–193.
- [31] C. SONG, J. CARDLE, AND K. LEUNG, *Transient mixed-flow models for storm sewers*, Journal of Hydraulic Engineering, ASCE, 109 (1983), pp. 1487–1503.
- [32] V. STREETER AND E. WYLIE, *Fluid transients in systems*, Prentice Hall, Englewood Cliffs, NJ, 1993.
- [33] D. WIGGERT, *Transient flow in free surface, pressurized systems*, Journal of the Hydraulics division, 98 (1972), pp. 11–27.
- [34] V. WINCKLER, *Logiciel belier4.0. Notes de principes*, technical report, EDF-CIH, Le Bourget du Lac, France, 1993.